Drivers of spatial variability in spring bloom onset and magnitude along a latitudinal gradient in the Nordic Seas

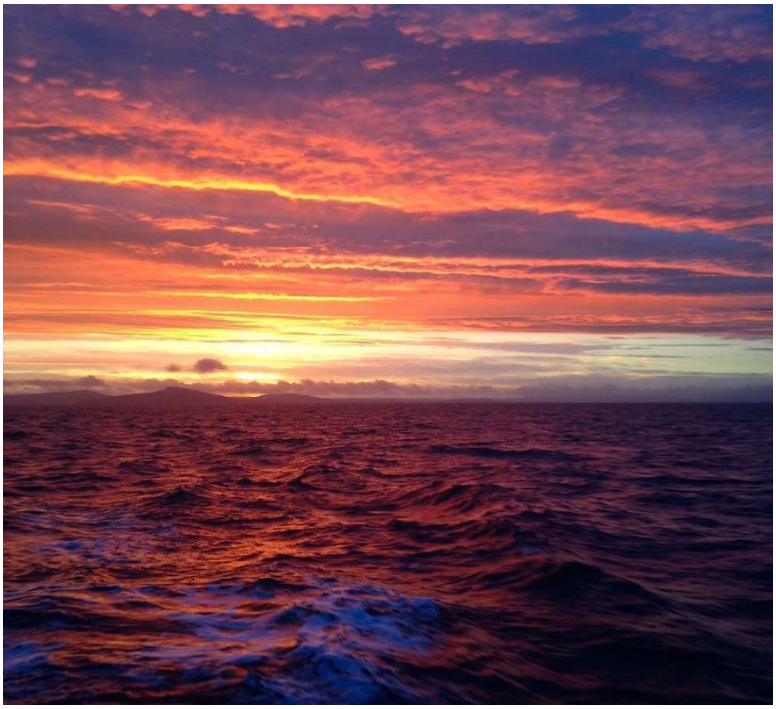

Thesis submitted in partial fulfilment of the requirements for the degree

Master of Science in Marine Biology

By

Elinor Tessin

Department of Biology

University of Bergen, Norway

May 2018

Abstract

Spring phytoplankton blooms in the Nordic Seas contribute a large proportion of global primary production, and their timing and magnitude heavily impacts higher trophic levels. Two key drivers of bloom development, stratification and irradiance, vary seasonally and with latitude. In this study, spring blooms along a latitudinal gradient in the Nordic Seas were observed in ocean color measurements and simulated in an idealized water column model with irradiance and vertical mixing (largely controlled by density stratification) as its main drivers. In both ocean color observations and simulations, a delay in spring bloom onset was observed south of 75°N. Phytoplankton dynamics in the idealized water column model were shown to be highly sensitive to turbulent diffusivity, a measure of vertical mixing highly dependent on stratification. Within a range of turbulent diffusivity, increased turbulent diffusivity led to delayed blooms with higher growth rates and magnitudes. At higher rates of mixing, population growth could not be sustained at the level required for a bloom, resulting instead in steady low-level phytoplankton concentrations. These results suggest that latitudinal variation in bloom timing can to a large degree be explained by latitudinal gradients of density stratification and irradiance.

Keywords: Spring bloom, phenology, phytoplankton, ocean color

1. Introduction

Marine primary production is dominated by phytoplankton. These single-celled algae are, unlike most autotrophs, not attached to substrate, but instead transported horizontally and vertically by currents and turbulence and therefore subject to a heavily fluctuating environment. They can only grow and reproduce within the sunlit upper layer of the ocean, but are limited by the rate at which nutrients can be replenished from below.

In large areas of the global ocean, low-level primary production is constantly taking place, but in other parts of the ocean, such as in high latitude, seasonal oceans, certain factors allow phytoplankton biomass to dramatically increase within short timespans. These blooms occur in coastal upwelling zones, but can also be a recurring feature in the open ocean, e.g. in spring in the temperate and sub-arctic Atlantic Ocean (Mann & Lazier, 2013).

Subject to intensive study since the 1920s, the North Atlantic spring bloom was first hypothesized to be initiated by seasonal increase of solar radiation, although this did not yet explain the large interannual variation in timing and magnitude of blooms, nor spatial variation along one latitude, nor the fact that blooms did not take place in various locations where irradiance should have been sufficient even in winter (Atkins, 1928; Marshall & Orr, 1928).

Gran and Braarud (1935) proposed that blooms are facilitated by stabilization of the water column through increased temperatures. In winter, heat loss at the surface and subsequent cold convection lead to a uniformly mixed layer from the surface down to depths where light is not sufficient for photosynthesis. Phytoplankton populations are circulated through this layer and do not spend enough time near the surface to significantly increase in numbers. The shallowing of that mixed layer through temperature stratification in spring then leads to increased exposure to light, stimulating growth and reproduction. This mechanism was further described and quantified by Sverdrup (1953), leading to a spring bloom theory that is, although repeatedly challenged, still widely accepted and taught today (Behrenfeld, 2010; Mann & Lazier, 2013).

Sverdrup's model described a water column with a uniformly mixed upper layer, in which light attenuation and turbulence are constant, and nutrients are not limiting phytoplankton growth. Phytoplankton cells are continuously circulated through this layer, subject to fluctuating light, and therefore ability to photosynthesize. Cell respiration, however, is assumed to be constant and independent of depth.

At a certain depth, irradiance provides enough energy for photosynthesis of a phytoplankton cell to exactly match respiration. A cell kept at this compensation depth could just survive, while below, it would either die or be forced to enter a vegetative state. However, turbulence and therefore constant circulation of cells allow cells mixed far below the compensation depth to grow and reproduce, if mixing depth does not exceed a critical depth at which respiration integrated over the water column is larger than integrated photosynthesis. In spring, critical depth increases with irradiance, while mixed layer depth decreases with increased density stratification, caused by formation of a temperature or salinity gradient (Sverdrup, 1953).

Because density stratification is not merely a function of solar heating but also heavily influenced by bathymetry and tides, wind stress and freshwater input, e.g. riverine runoff with increased snowmelt in spring, or melting of sea ice, this model can be reconciled with the interannual and spatial variation of algal blooms observed in reality (Talley et al., 2011).

Additionally, as critical depth decreases with increasing light attenuation in the water column, potential for photosynthesis is not estimated only from surface irradiance as in previous concepts.

Certain assumptions of Sverdrup's model, e.g. the homogeneous distribution of phytoplankton cells and grazers through the mixed layer, are unlikely to be observed in situ. Several reports of spring blooms occurrences in unstratified waters have led to the model being challenged (Colebrook, 1979; Eilertsen et al., 1995; Townsend et al., 1992). Huisman et al. (1999) proposed that not only the mixing depth, but also the intensity of mixing must be accounted for. Even if mixing depth exceeds critical depth, a bloom could still take place if the turbulence

within the mixed layer remained below a critical turbulence. Behrenfeld (2010) later disputed the importance of mixed layer shoaling for bloom initiation, instead suggesting that concentrating plankton within a thinner mixed layer led to increased grazing and inhibited blooms.

Still, the general pattern of thorough mixing followed by stratification holds true for most major bloom events. Permanently stratified tropical and subtropical regions do not experience large variations in primary production, while chlorophyll concentrations in the North Atlantic and North Pacific do not only reach the highest global maxima during spring blooms, but are also highest when averaged over a decade (Racault et al., 2012).

Seasonality, through disrupting the balance between nutrient depletion and replenishment as well as biomass accumulation and grazing, therefore seems to, at least intermittently, benefit primary production, which leads to the question how more extreme seasonality at high latitudes might further impact primary production. Above the Arctic circle at 63°N, solar radiation is unavailable during the Polar night, while midnight sun allows for continuous photosynthesis during summer. Stratification in subpolar and polar regions is usually salinity rather than temperature-driven, especially in zones that are seasonally ice-covered. Thermoclines remain weak, or do not form at all (Talley et al., 2011).

Based on these differences in seasonality, Longhurst (1998) proposed a division of the Nordic Seas into two categories: a westerlies biome with a mid-latitude seasonal cycle exhibiting an early spring and an autumn bloom, and a polar biome with a single midsummer bloom. This dichotomous view of polar and mid-latitude seasonal production cycles has largely prevailed, although constant exchange of water masses and organisms between biomes as well as gradual change of environmental characteristics means that no exact borders can be drawn. Instead, in a large region between mid-latitude and high latitude oceans, blooms occur on a gradient between these two extremes.

Cushing (1959) introduced the concept of a northward delay of spring blooms, based mainly on the latitudinal irradiance gradient. Empirical studies recorded such a delay in bloom onset in the North Atlantic between 40° and 70° N, coinciding with the seasonal increase in thermal stratification (Colebrook, 1979; Strass & Woods, 1988). However, they also observed early blooms at high latitudes within that range, ascribed to high salinity stratification.

Several studies have since expanded on this phenomenon using satellite ocean color data. Siegel (2002) found a delay of spring bloom onset of ca. 6 days per degree latitude between 35°N and 50°N in the Atlantic, but no clear trend from 50°N to 75°N. Studying the Greenland Sea, Wu et al. (2008) found a delay of 4 days per degree latitude between 40 and 60°N, and blooms between 60 and 75°N occurring at the same time as those at 40°N in beginning of April. They succeeded in replicating this pattern in a model forced with estimates of mixed layer depth, suggesting that strong salinity stratification due to sea ice melting and land run-off in the northern part of their study area reduces mixing and allows early bloom formation.

With sea ice reduction, increased temperature, and altered wind and precipitation patterns, climate change is likely affecting bloom timing, and without the entire marine food web. Phytoplankton constitute the bottom of the oceanic food web, and life cycles events of grazers in the Nordic Seas are attuned to their blooms (Broms & Melle, 2007; Vikebø et al., 2012). Disruption of the synchronization between blooms and life events of grazers affects species at higher trophic levels, including fish species exploited for human consumption (Cushing, 1990).

To contribute to a better understanding of drivers of variability in bloom timing, this study will investigate the timing of spring bloom onset and magnitude along a latitudinal gradient from 60°N to 80°N in the Nordic Seas by analyzing satellite chlorophyll estimates. Further, I will attempt to identify which drivers cause latitudinal variability through modelling of phytoplankton growth dynamics. I hypothesize that a latitudinal bloom timing pattern observed in ocean color data can be reproduced in an idealized water column model driven primarily by variation in solar radiation and density stratification.

2. Material & Methods

2.1. Study area

This study examined and simulated phytoplankton concentrations along a latitudinal gradient in the Nordic Seas from March to June.

The Norwegian, Greenland, Iceland and Barents Seas, together referred to as the Nordic Seas, are influenced by both North Atlantic and Arctic water masses. They are separated from each other by submarine ridges and therefore each constitute a circulation system of their own. The Barents Sea, a shallow shelf area, as well as the deep Fram Strait are the main areas of water exchange between these seas and the Arctic Ocean and contribute ca. 90% of all water entering the Arctic Ocean. Exchange with Atlantic water takes place through the Denmark Strait, the Faroe-Iceland Ridge and the Faroe-Shetland Channel. The amount of warm, saline Atlantic water entering the Arctic through the Nordic Seas determines climate and circulation as well as extent of sea ice in the region (Korablev et al., 2014).

Nine study locations were chosen along a latitudinal gradient on 0.125°E, ranging from 60.125°N to 80.125°N in 2.5° intervals (Figure 1). The two southernmost stations are located on the North Sea shelf and slope, while all other stations are situated in the deep sea. Only the southernmost station included coastal areas. The physical and chemical environment at these stations is to a large extent determined by the presence of two water masses, Atlantic and Polar Water. Atlantic Water with temperatures around 7°C and salinity >35 dominates in most of the Norwegian Sea, with temperature and salinity decreasing northward (Levitus et al., 2013). Northern North Sea Water is also influenced by Atlantic Water, resulting in salinities around 35 and medium to low nutrient concentrations (Laevastu, 1962). At the locations in the Greenland Sea, the influence of Polar Water with temperature <0°C and salinity <34 increases (Blindheim & Østerhus, 2005). Atlantic phosphate concentrations range from 0.4 mmol m^{-3} in the upper water column to 1.2 mmol m^{-3} at greater depths, while nitrate concentrations increase

from around 6 mmol m^{-3} in the upper 150 m up to 18 mmol m^{-3} in the deep sea. Nutrient concentrations in the North Sea are generally slightly higher (Garcia et al., 2013).

The circulation of these water masses is determined by bathymetric features, with the Atlantic Current (AC) flowing northward along the Norwegian shelf break and the East Greenland Current (EGC) transporting Polar water southward along the Greenland shelf break. A branch of the EGC flows around the Greenlandic Basin, where stations 6 and 7 are located, while the AC is constrained to east of the Mohn Ridge (72.5°N, 5°E). The northernmost station in the middle of the Fram Strait is again influenced by both water masses.

These study locations were chosen according to data availability; ocean color data of locations further north did not yield enough information for comparison with simulated data due to high solar zenith angles throughout spring as well as ice and cloud cover.

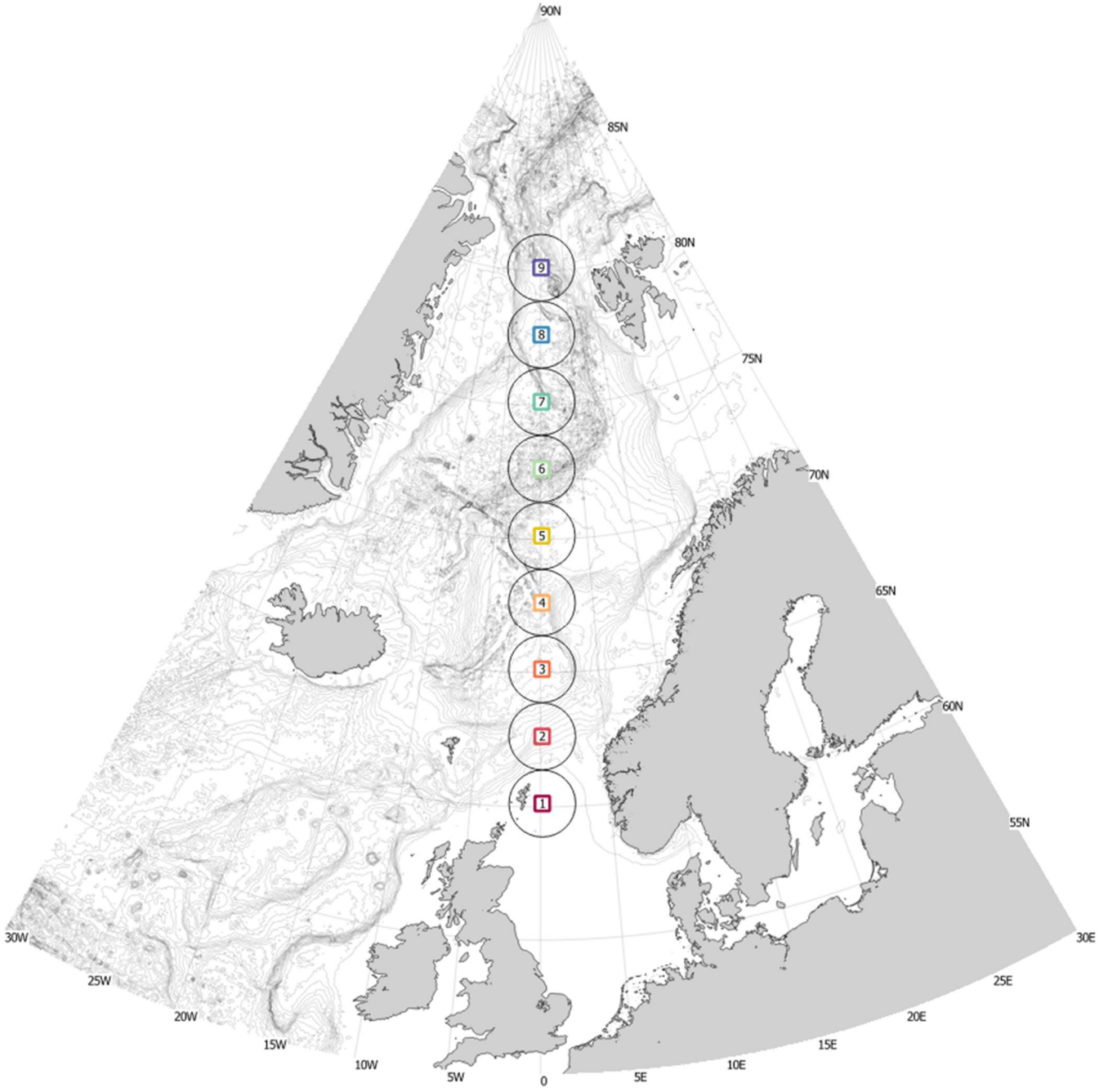

Figure 1: Map of the study area showing bathymetric features. Study locations on a latitudinal gradient along 0.125°E are labelled. Circles with a radius of 138.75 km (1.25°) around each station depict the area from which ocean color and density data were extracted.

2.2. Ocean Color Data

Concentrations of chlorophyll a were used as a proxy for phytoplankton biomass and derived from remote sensing ocean color data.

The wavelengths constituting ocean color, or water-leaving radiance, differ according to the concentration of particles present in the water column. In clear seawater, higher wavelengths are most strongly absorbed, resulting in blue upwelled light. Chlorophyll a absorbs both red and blue strongly while other wavelengths are scattered; if phytoplankton concentrations in the upper 25 m of the water column are high, the water-leaving radiance will therefore consist mostly of wavelengths in the green region of the visible spectrum (Robinson, 2004).

Ocean color sensors are composed of optical bands measuring water-leaving radiance in red, green, and blue wavelengths (the wavelengths chosen to represent these regions of the spectrum differ slightly between sensors). The relationship between chlorophyll a concentrations in seawater and the ratio of radiance measured by the green band versus the other bands has been empirically determined (O'Reilly et al., 1998).

The ESA ocean color dataset (accessed at www.globcolour.info) is a composite of data from different NASA and ESA sensors starting in 1997, with a spatial resolution of 1/24° (4.63 km at the equator).

8-day composites of level 3 data, meaning calibrated, time- and georeferenced satellite measurements, between 1998 and 2012 were analyzed and averaged for each 8-day period between year days 57 and 183. This data originated from the Sea-viewing Wide Field of View Sensor (SeaWiFS, 1998-2010), the Moderate Resolution Imaging Spectroradiometer on the Aqua satellite (MODIS, May 2002-2012), Medium Resolution Imaging Spectrometer (MERIS, June 2002 - April 2012) and Visible and Infrared Imaging/Radiometer Suite (VIIRS, 2012) sensors. The time range between 1998 and 2012 was chosen to not exceed the range for which density data of the study area was available (see section 2.3.5.2).

The algorithm used to produce the Level 3 composites is valid for case 1 waters, where chlorophyll is expected to be more abundant than inorganic particles, therefore excluding coastal areas. Data from different sensors were merged according to the GSM (Garver-Siegel-Maritorena-Model) method, which uses the normalized reflectances at original sensor wavelengths without intercalibration. Merging increases temporal and spatial availability of data, but differences in design and accuracy between the sensors must be considered. Alternatives to the GSM method are simple averaging of final single sensor products and weighted averaging (AVW), where products are weighted by each sensor's relative error. Using the original remote-sensing reflectances to merge sensor outputs, as in the GSM method, allows for the use of a single biooptical algorithm to determine chlorophyll concentrations rather than merging data produced using different algorithms (Maritorena & Siegel, 2005).

Downloaded data was stored in netCDF-4 files and first visualized in Panoply (Version 4.8.3), then analyzed in R (Version 3.4.1) using RStudio (Version 1.1.383). To manipulate the netCDF-4 files, packages *ncdf* (Version 1.16) and *raster* (Version 2.6-7) were used.

Pixels within a 138.75 km (1.25°) radius of each of the nine stations were averaged for 8-day periods across years. This distance threshold was chosen to ensure maximum data availability while preventing overlap between stations. The number of valid pixels and standard deviation of chlorophyll concentrations within these areas were recorded.

2.3. Modelling of spring phytoplankton dynamics

The results of the ocean color analysis were compared with predictions from an idealized water column model. Two physical factors, mixing and solar radiation, were assumed as the main drivers of latitudinal differences in bloom timing in the model.

2.3.1. Water column model of Huisman et al. (2006)

The model used to predict bloom timing is a slightly modified (2.3.4) version of the Huisman model. It describes the dynamics of phytoplankton cell densities (*P*) and nutrient concentrations (*N*) in a water column (Huisman et al., 2006). Cell concentrations change over time due to growth and loss and are moved through the water column due to sinking and mixing.

The specific growth rate, which is assumed to follow the Monod equation, is dependent on and limited by either nutrient availability (*N*) or light intensity (*I*) according to Von Liebig's law of the minimum. The maximum specific growth rate (μ_{max}), as well as the half-saturation constants for growth limited by light intensity or nutrient availability (H_I, H_N), are empirically determined values and taken from Huisman et al. (2006).

Equation 1: Specific growth rate of phytoplankton

$$\mu(N,I) = \mu_{max} \cdot \min\left(\frac{I}{H_i + I}, \frac{N}{H_N + N}\right)$$

Light intensity in the water column decreases exponentially with depth following Lambert Beer's law. Light incident at the surface (I_{in}) was modelled using the "Astrocalc4R" function in the fishmethods R package (Version 1.10-4) (see section 2.3.5).

Light attenuation in the water column consists of background light attenuation (K_b) and light attenuation due to phytoplankton, with K_I as the specific light absorption coefficient of phytoplankton and σ as the integration variable describing the non-uniform distribution of phytoplankton (P) in the water column.

Equation 2: Light at depth

$$I = I_{in}\exp(-K_b z - K_1 \int_0^z P(t,\sigma)d\sigma)$$

To describe the resulting net growth, mortality (m) must be accounted for. Cells sink with velocity v, but can also be mixed up- and downwards according to the vertical turbulent diffusivity (κ). The local change in phytoplankton concentrations ($\frac{dP}{dt}$) at depth z is then a function of growth, mortality, and losses or gains due to mixing and sinking of cells from depths above and below:

Equation 3: Dynamics of phytoplankton cell concentrations

$$\frac{dP}{dt} = (\mu(N,I) - m)\,P - v\frac{dP}{dz} + \kappa\frac{d^2P}{dz^2}$$

Nutrient concentration dynamics in the water column can be described similarly; the uptake of nutrients depends on the phytoplankton growth rate, with α as the nutrient content of one cell. Unlike phytoplankton cells, nutrients do not sink in the water column, but are affected by mixing (κ). Mortality (m) of phytoplankton cells also affects nutrient concentrations, as a proportion (ε) of the nutrient content of cells (α) is recycled.

Equation 4: Dynamics of nutrient concentrations

$$\frac{dN}{dt} = -\alpha\mu(N,I)P + \varepsilon\alpha mP + \kappa\frac{d^2N}{dz^2}$$

2.3.2. Numerical solution

The model as written by Huisman et al. (2006) consists of two partial differential equations (Equation 3, Equation 4). It was adapted into a numerical solution by setting a finite number of depth and time steps (Table 1) and run in Matlab (R2017a, Appendix 4).

The length of time steps was set to the maximum value allowing the numerical solution to converge. A simulation period of 128 days comprised of 182880 time steps was chosen to match the 16 8-day composites of ocean color data selected for analysis.

Table 1: Parameters of the numeric solution of the model adapted from Huisman et al. (2006).

Parameter	Symbol	Value	Unit
Number of depth cells	*z*	300	-
Length of a depth cell	*dz*	1	m
Number of time steps	*t*	182880	-
Length of a time step	*dt*	60	s

2.3.3. Initial and boundary conditions

The model was used to simulate a spring bloom rather than reach a steady state as in Huisman et al. (2006). Initial conditions were therefore chosen to represent a typical early spring pre-bloom situation with a thoroughly mixed water column, and uniformly low phytoplankton and high nutrient concentrations. Initial phytoplankton (*P*) and nutrient concentrations (*N*) in all depth cells were respectively set to 0.01 and 10 mmol N m^{-3} in all depth cells. Nutrients are assumed to be constantly replenished at the bottom of the water column, but there is no exchange through the surface.

2.3.4. Model modifications

Nitrogen is generally considered to be the limiting nutrient in marine ecosystem and was accordingly chosen as the model currency (Howarth, 1988). In Huisman et al. (2006), nitrogen was converted to cell number using a fixed cellular nitrogen concentration (α, Table 2). Phytoplankton concentrations in this version of the model were internally given in mmol N m^{-3}, the same unit as nutrient concentrations, but to ease comparison with ocean color chlorophyll concentrations, the output was then converted to mg Chl m^{-3}, rather than cells m^{-3} as in Huisman et al. (2006).

The conversion factor of 0.63 mmol N m^{-3} per mg Chl m^{-3} consists of 6.625, the ratio of carbon to nitrogen (Redfield, 1958) multiplied with 12 mg mol^{-1}, the molecular weight of carbon, divided by 50, the ratio of carbon to chlorophyll (Wienke & Cloern, 1987).

Self-shading in the original model is determined by a single light absorption coefficient (K_1), amounting to a linear relationship between chlorophyll concentration and light absorption. While this might be valid for the oligotrophic conditions and low phytoplankton concentrations simulated in Huisman et al. (2006), it does not sufficiently describe self-shading at the high chlorophyll concentrations present during a spring bloom.

Morel (1988) instead described the increase of attenuation with chlorophyll concentrations as a power function with values for coefficient K_1 (0.121) and exponent K_2 (0.428) based on empirical evidence. Phytoplankton specific light attenuation (K_P) increases successively less with increased chlorophyll concentrations (Chl):

Equation 5: Phytoplankton-specific light attenuation (Morel 1988)

$$K_P = K_1 Chl^{K_2}$$

Chlorophyll concentrations (Chl) in Morel (1988) are measured in mg Chl m^{-3}, while the model used in this study describes phytoplankton concentration dynamics using a unit of mmol N m^{-3}. Applying the conversion factor of 0.63 mmol N m^{-3} per mg Chl m^{-3} (derived above) in Equation 5 produces a K_1 value of 0.19.

All other parameter values of the model were kept as in Huisman et al. (2006) (Table 2).

Table 2: Parameters used in the model. All parameters except those marked with * are taken from Huisman et al. (2006) without changes.

Parameter	Symbol	Value	Unit
Background light attenuation*	K_b	0.045	m^{-1}
Nutrient content of a phytoplankton cell	α	1 e^{-9}	mmol N $cell^{-1}$
Maximum growth rate	μ_{max}	1.11 e^{-5}	s^{-1}
Loss rate	m	2.78 e^{-6}	s^{-1}
Half saturation irradiance	H_i	20	µmol photons m^{-2} s^{-1}
Half saturation nutrient	H_n	0.025	mmol m^{-3}
Light absorption coefficient of phytoplankton*	K_1	0.14	m^2 mmol N^{-1}
Light absorption coefficient of phytoplankton*	K_2	0.428	-
Cell sinking velocity	v	1.17 e^{-5}	m d^{-1}
Nutrient recycling coefficient	ε	0.5	-
Vertical turbulent diffusivity*	κ	-	m^2 s^{-1}
Surface light*	I_{in}	-	µmol photons m^{-2} s^{-1}

2.3.5. Environmental variables

Environmental forcing in the model consisted of solar radiation and turbulent diffusivity. To simulate a seasonal environment, turbulent diffusivity and surface light were described as vectors varying throughout the simulation period.

2.3.5.1. Irradiance

Photosynthetically active radiation (PAR) was simulated hourly for the chosen locations and study period of March to June using a model developed by Frouin et al. (1989), which considers solar zenith angle as well as scattering by aerosols to compute PAR at ocean surfaces (Jacobson et al., 2011). The model was applied for the nine stations using the "Astrocalc4R" function in the fishmethods R package (Version 1.10-4). Function output was converted from W m^{-2} to µmol photons m^{-2} s^{-1} using a conversion factor of 4.57 (Thimijan & Heins, 1983).

Cloud cover was not accounted for. To fit with the model's timesteps of 60 seconds, hourly irradiance values were interpolated.

2.3.5.2. Density stratification and turbulent diffusivity

Temperature and salinity profiles were obtained from the World Ocean Atlas (WOA, Levitus et al., 2013). The datasets included profiles averaged for each month of the year, measured between 1955 and 2012. Measurements in the dataset are interpolated to standard depths (5 m steps between 0-100 m depth; 25 m steps between 100-500 m depth). The dataset has a spatial resolution of 1/4°.

Density was computed from temperature and salinity using the "swRho" function in the oce R package (Version 0.9-23). One density profile for each station was averaged from all profiles with depths >150 m taken within 138.75 km of that station.

To derive a measure of density stratification and vertical mixing from these profiles, buoyancy frequency (N) and turbulent diffusivity (κ) were calculated.

The buoyancy or Brunt-Väisälä frequency (N) is computed from the change of density (r) over depth (z) and acceleration due to gravity (g) divided by reference density r_0 (Mann & Lazier, 2013). It describes the frequency of the oscillation resulting from the vertical displacement of a water parcel in a water column, which depends on the density stratification in that water column. The greater the density gradient, the stronger are the forces returning that water parcel to its original place, a water layer of equal density. A strongly stratified water column will result in a high buoyancy frequency (Talley et al., 2011).

Equation 6: Buoyancy frequency

$$N = \sqrt{(\frac{g}{r_0})(\frac{dr}{dz})}$$

In the model by Huisman et al. (2006), the mixing of phytoplankton and nutrients through the water column depends on the turbulent diffusivity (κ). Vertical turbulent diffusion is reduced with increased density stratification, and increased with energy input, e.g. due to wind stress. Deriving a realistic estimate of turbulent diffusivity is not trivial, and its effect on phytoplankton and nutrient concentration dynamics was mainly investigated by performing a sensitivity analysis (see section 2.3.6).

Li et al. (1984) estimated a global average value of $1.7 \cdot 10^{-4}$ m^2 s^{-1} for vertical mixing through the oceanic thermocline based on tritium distributions. This was chosen as the medium value of a range of turbulent diffusivities in a sensitivity analysis (see section 2.3.6).

Sundby (1983), using fish egg distributions to compute turbulent diffusivity of the mixed layer in the North Sea and Norwegian Sea, empirically derived the following relationship between turbulent diffusivity and wind speed (w), valid for wind speeds between 0 and 12 m s^{-1}:

Equation 7: Turbulent diffusivity as a function of wind speed

$$\kappa = 76.1 \cdot 10^{-4} + 2.26 \cdot 10^{-4} \cdot w^2$$

Applying this relationship to an average wind speed of 11 m s^{-1}, calculated from NOAA satellite wind speed measurements (H.-M. Zhang et al., 2006) for the area examined in the present study, results in a turbulent diffusivity of 0.0349 m^2 s^{-1}. This value was also incorporated in the sensitivity analysis (see section 2.3.6).

Denman & Gargett (1983) describe turbulent diffusivity as a function of buoyancy frequency (*N*) and energy dissipation rate (*e*):

Equation 8: Turbulent diffusivity as a function of buoyancy frequency

$$\kappa = 0.25 * e * N^{-2}$$

The dissipation rate of kinetic energy (*e*) is related to wind strength (Denman & Gargett, 1983; Mann & Lazier, 2013). In the present study, a constant wind speed (*W*) of 11 m s^{-1}, averaged for the study area as described above, was assumed for all stations.

The values used for constants a_1 ($4.9 \cdot 10^{-9}$ m^{-1}) and a_2 ($4.23 \cdot 10^{-8}$ m^2 s^{-3}) are estimates taken from a linear regression fitted to measurements of *e* at different wind speeds (Table 4 in Aksnes & Lie, 1990, who based the calculations on Denman & Gargett, 1983).

Equation 9: Dissipation rate of kinetic energy

$$e = a_1 W^3 + a_2$$

An average turbulent diffusivity of the upper 125 meters of the water column was approximated from Equation 8 for each month of the study period (March – June). To fit the timesteps of the model, linear interpolation was applied.

2.3.6. Sensitivity analyses

Three sensitivity analyses were performed to examine the effects of irradiance, turbulent diffusivity and background attenuation on model results. Phytoplankton and nutrient concentration dynamics were modelled in a 300 m water column adjusting one factor while keeping all others constant.

For irradiance, light regimes modelled for three different locations throughout spring were compared while keeping all other factors constant. For turbulent diffusivity, $1.7 \cdot 10^{-4}$ m^2 s^{-1} was chosen (estimated as an average value for vertical mixing through the oceanic thermocline in Li et al., 1984, based on tritium distributions).

The effect of turbulent diffusivity on the model output was examined using 600 µmol photons m^{-2} s^{-1} as a constant value for surface light, as in Huisman et al. (2006). Four levels of turbulent diffusivity were compared: $1.7 \cdot 10^{-4}$ m^2 s^{-1} (considered average by Li et al., 1984), values an order of magnitude above and below ($1.7 \cdot 10^{-5}$ m^2 s^{-1}; $1.7 \cdot 10^{-3}$ m^2 s^{-1}), and $3.49 \cdot 10^{-2}$ m^2 s^{-1}, the turbulent diffusivity derived from an average wind speed in the study area, using Equation 7.

The background attenuation coefficient (i.e. non-chlorophyll attenuation) chosen for the simulations (0.045 m^{-1}) is the same as in the original study by Huisman et al. (2016). Norheim et al. (2016) measured an average light attenuation coefficient (background and chlorophyll attenuation) of 0.063 m^{-1} for PAR in the Norwegian sea in spring with chlorophyll concentrations less than 1 mg m^{-3} (DL Aksnes, personal communication, February 23, 2018). Keeping turbulent diffusivity ($1.7 \cdot 10^{-4}$ m^2 s^{-1}) and surface light (600 µmol photons m^{-2} s^{-1}) constant, the model output for both values was compared.

2.4. Bloom timing

To offer a wide perspective of bloom timing and facilitate comparison with previous studies, six methods of characterizing bloom timing were utilized in the present study.

Bloom maxima were identified as in Kahru et al. (2011) and Platt et al. (2003) (Bloom maxima method).

As an alternative also accounting for secondary peaks, the center of gravity beneath each timeseries was calculated. Edwards et al. (2004) used the center of gravity of zooplankton timeseries to detect seasonal peaks using the following equation:

Equation 10: Identifying the center of gravity of a timeseries (Edwards et al., 2004)

$$T = \frac{\sum_1^{12} M \cdot x_m}{\sum_1^{12} x_m}$$

With T as the date corresponding to the center of gravity of the area below a timeseries, M as the month, and x_m as the mean chlorophyll concentration of that month. For the purposes of this study, M was replaced by the index of 8-day intervals between March and June, and x_m by the mean chlorophyll concentration of these intervals (Center of gravity method).

Bloom onset has been defined in many ways, but a common approach is to define a threshold concentration. Wu et al. (2008) simply define bloom onset as the first day with chlorophyll concentrations exceeding 1 mg m^{-3} (1 mg threshold method).

Brody et al. (2013) describe two methods of detecting bloom onset based on dynamic thresholds. A threshold concentration of 5% above the median chlorophyll concentration was used to identify bloom onset as shown in Siegel et al. (2002) and Henson et al. (2006) (Median threshold method). Further, the day on which cumulative chlorophyll concentration exceeded 15% of the maximum chlorophyll concentration was used to identify bloom onset as described by Greve et al. (2001) and Mackas et al. (2012) (Cumulative sum method). The median threshold method is more likely to identify bloom onset as the largest increase in biomass preceding a peak, while the cumulative sum method with the chosen threshold detects initial increases in biomass (Brody et al., 2013).

The resulting bloom timing dates of different latitudes were evaluated by computing Pearson correlation coefficients, Spearman rank correlation coefficients and corresponding p-values. Pearson correlation coefficients take values between -1 and 1 depending on whether a linear and negative or positive relationship is measured. Spearman rank correlation coefficients can also take a value of 1 or -1 if the measured relationship is non-linear, if it is monotonic. The corresponding p-value then states whether the correlation is significantly different from zero ($p > 0.05$).

2.5. Comparison of ocean color and simulated bloom observations

The layer of the ocean visible to remote sensors corresponds to approximately the first optical depth of the water column, in which irradiance decreases to 1/e of surface irradiance (Gordon & McCluney, 1975). Following Beer's law (Equation 2), this depth is found at 1/K. For clear ocean water without attenuation due to chlorophyll, with a K_b of 0.045 m^{-1} (Table 2), this is at 22.2 m. Other authors mention penetration depths of 25 m for oligotrophic ocean water (André, 1992; R.-H. Zhang et al., 2011). As an approximation of the depth range theoretically visible to remote sensors and to facilitate comparison with ocean color observations, the upper 25 m of the modelled water column were therefore used to characterize bloom timing in the simulation.

3. Results

3.1. Ocean color bloom observations

Chlorophyll concentrations at all stations increased during spring, although at different rates and to different magnitudes (Figure 2). The highest bloom magnitude, but also largest interannual variation in magnitude was observed at station 7 (Figure 3).

No clear relationship between bloom magnitude and latitude was found (Figure 3). Maximum chlorophyll concentrations were larger at the southern and northern stations compared to stations in the middle of the latitudinal gradient. Variability of maximum concentrations was larger at the northern stations.

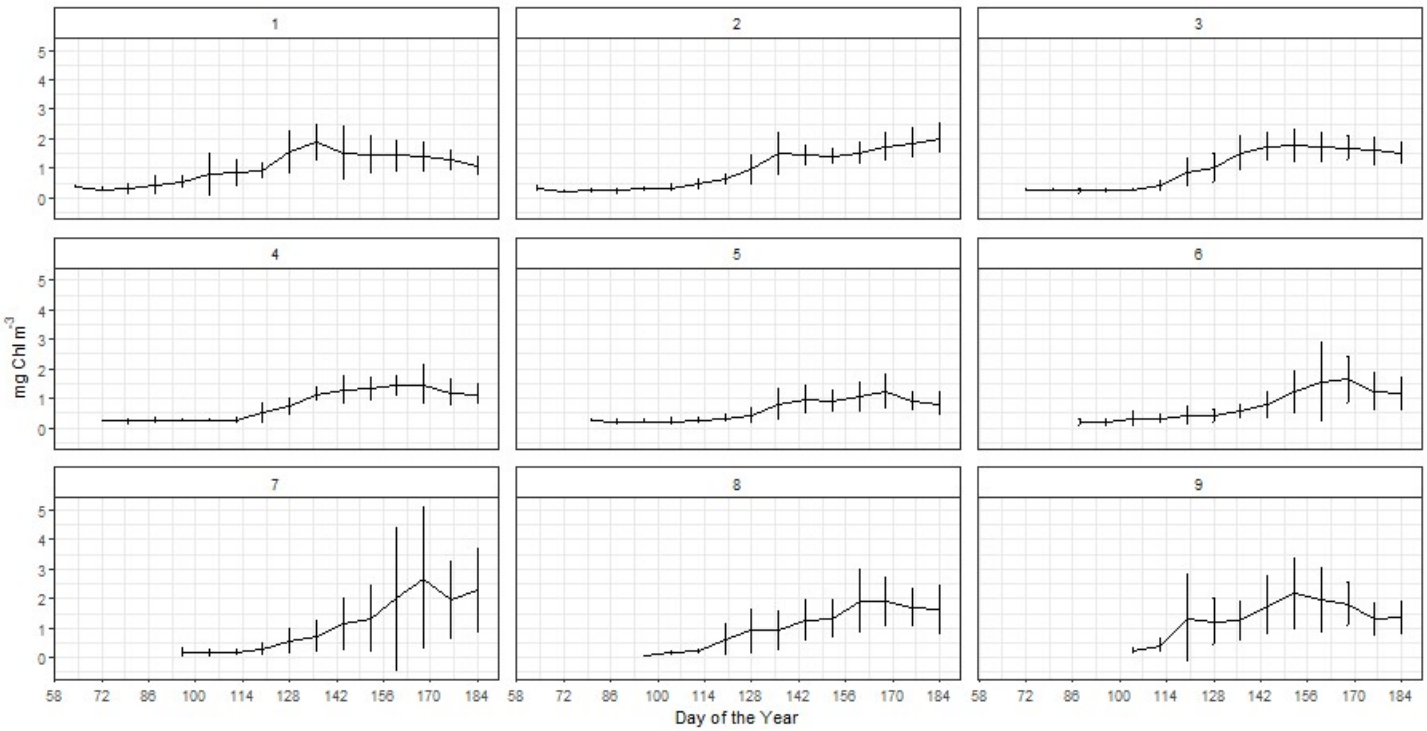

Figure 2: Ocean color chlorophyll timeseries for stations 1-9 (with station 1 as the southernmost). Pixels within a radius of 138.75 km (1.25°) of the station coordinates were binned and averaged for 8-day intervals between 1998 and 2012. Bars show standard deviations of binned chlorophyll concentrations between years. Time is given as day of the year, with January 1st as day 1.

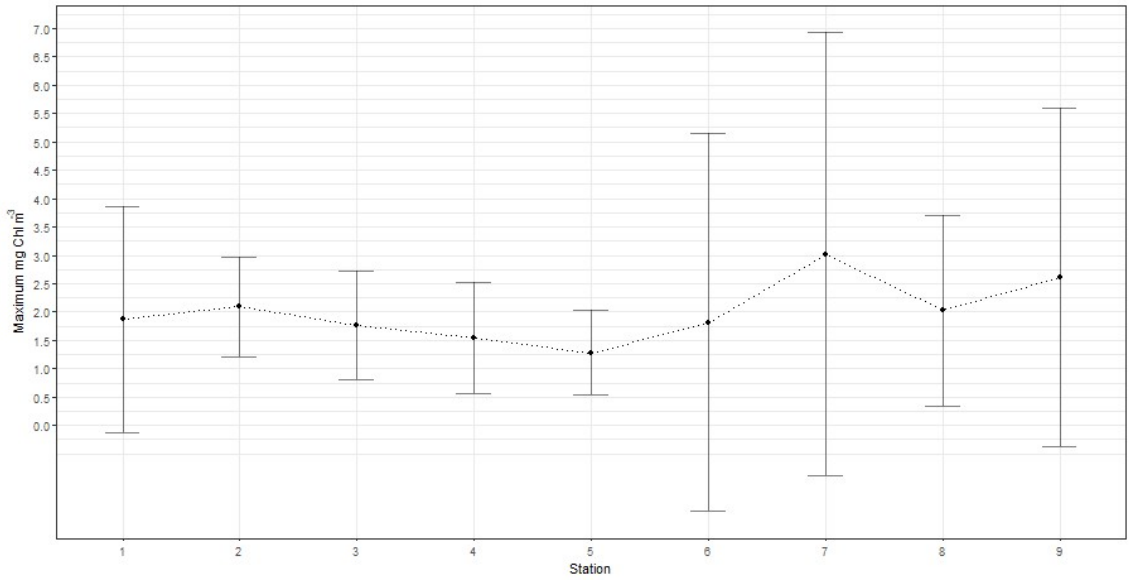

Figure 3: Maximum chlorophyll concentrations of the stations 1-9 (south to north) from timeseries averaged for 8-day intervals between 1998 and 2012. Error bars show standard deviations of binned chlorophyll concentrations between years.

3.1.1. Bloom timing

Bloom onset and maxima at all stations occurred within a time period of 84 days (Figure 4). On average, bloom onset was delayed by 2 days between stations. Between stations 1 and 7, the delay was 4 days per station. Blooms north of station 7 occurred on the same day according to the median threshold method, and on average 8 days and 4 days earlier according to the center of gravity and cumulative sum methods.

Bloom maxima dates did not show a clear latitudinal pattern, although the southernmost station peaked first.

Pearson and Spearman correlation tests showed strong correlation between station number and bloom onset as detected by the Median Threshold and Cumulative Sum method.

For all methods, correlation increased when disregarding stations 8 and 9. This did not change statistical significance.

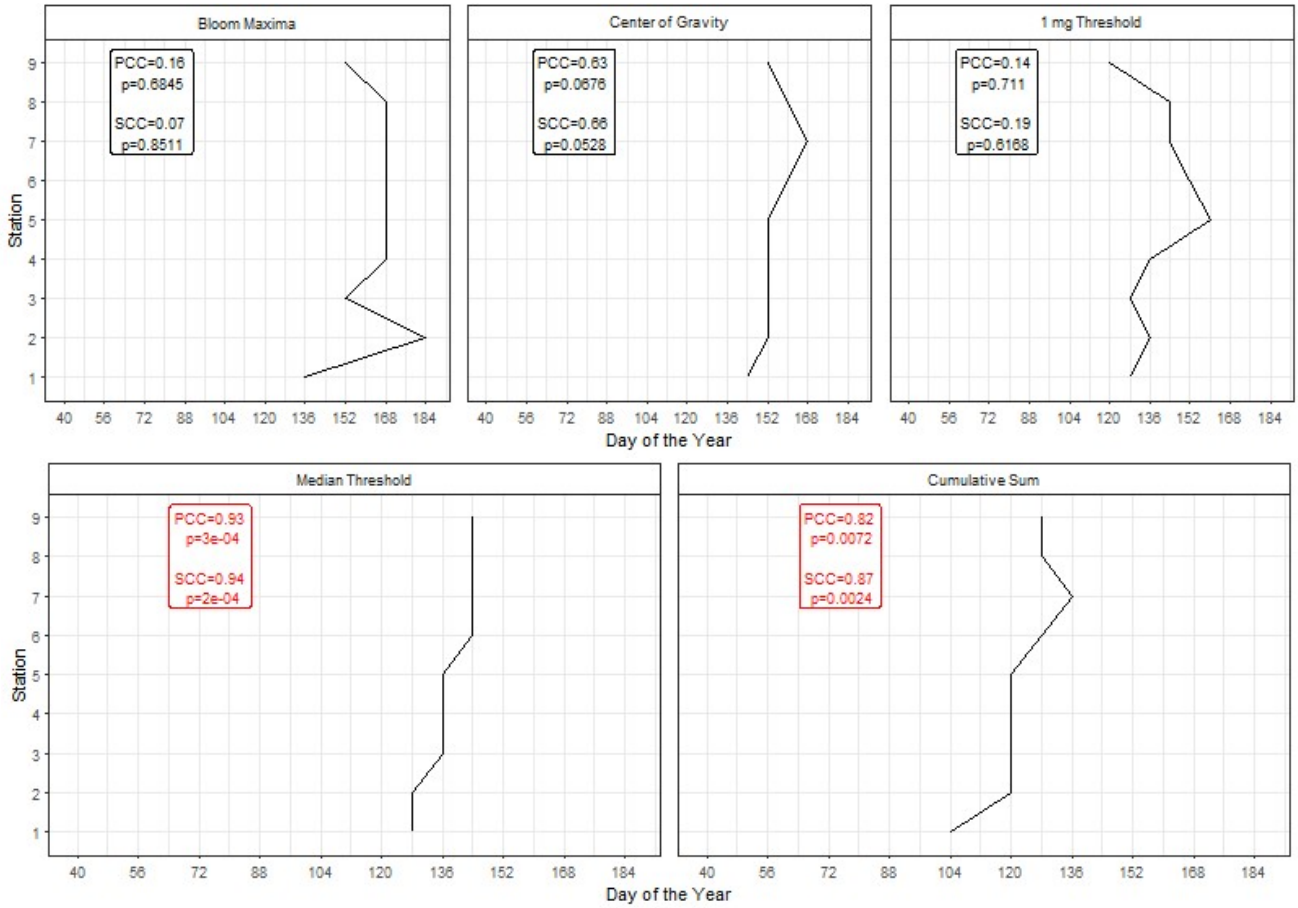

Figure 4: Bloom dates of ocean color chlorophyll timeseries, as identified by five different methods, plotted against station number. Labels contain Pearson Correlation Coefficient (PCC), Spearman Rank Correlation Coefficient (SCC) and corresponding p-values, with statistically significant values ($p<0.05$) marked in red. Time is given as day of the year, with January 1st as day 1.

3.2. Irradiance

Photosynthetically active radiation was modelled from February 26th (day 57) to July 4th (day 183) (Figure 5).

As the model did not consider effects of cloud cover, irradiance is purely a function of solar position. At the start of the simulation period, mean irradiance per day decreases with increasing latitude, and station 9 is still experiencing polar night. On spring equinox, days are equally long at all stations, but mean irradiance per day is higher at stations further south due to higher angles of incident sunlight.

Stations 4-9 are north of the Arctic circle and all experience midnight sun by summer solstice (June 20th; day 171). Incident sunlight still arrives at lower angles at stations further north, but longer days at these stations lead to higher values of mean daily irradiance.

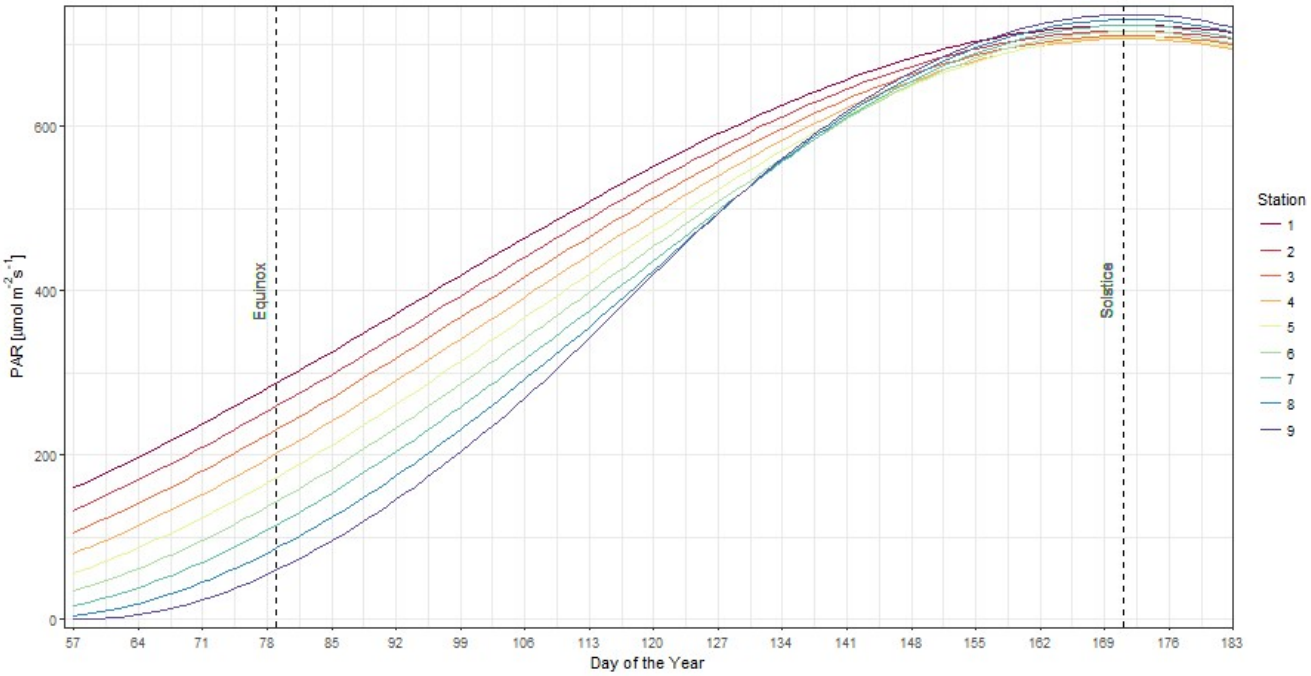

Figure 5: Mean photosynthetically active irradiance per day in µmol m^{-2} s^{-1} modelled from February 26th (day 57) to July 4th (day 183) for nine stations, using the Astrocalc4R function (Jacobson et al., 2011). Irradiance was modelled hourly, but is here plotted as mean irradiance per day for ease of viewing. Equinox on March 20th (day 79) and summer solstice on June 20th (day 171) are marked.

3.3. Density stratification

Density profiles varied the strongest between months at station 1 and 9 (Figure 6). This was due to an increase in surface temperature at station 1, and a decrease in surface salinity at station 9 (Appendix 2, Appendix 3).

Stations 5 to 7 showed very little variation between months, with slightly higher density gradients at the end of spring, but no pycnocline formation.

The difference between density at 125 m depth and the surface, an indicator of stratification, increased at all station between March and June (Figure 7). In March, stratification was low at all stations. The strongest stratification and also highest seasonal increase in stratification was observed at station 9. Here, stratification increased from March to April, slightly decreased until May, then reached a maximum density difference of 1.5 in June.

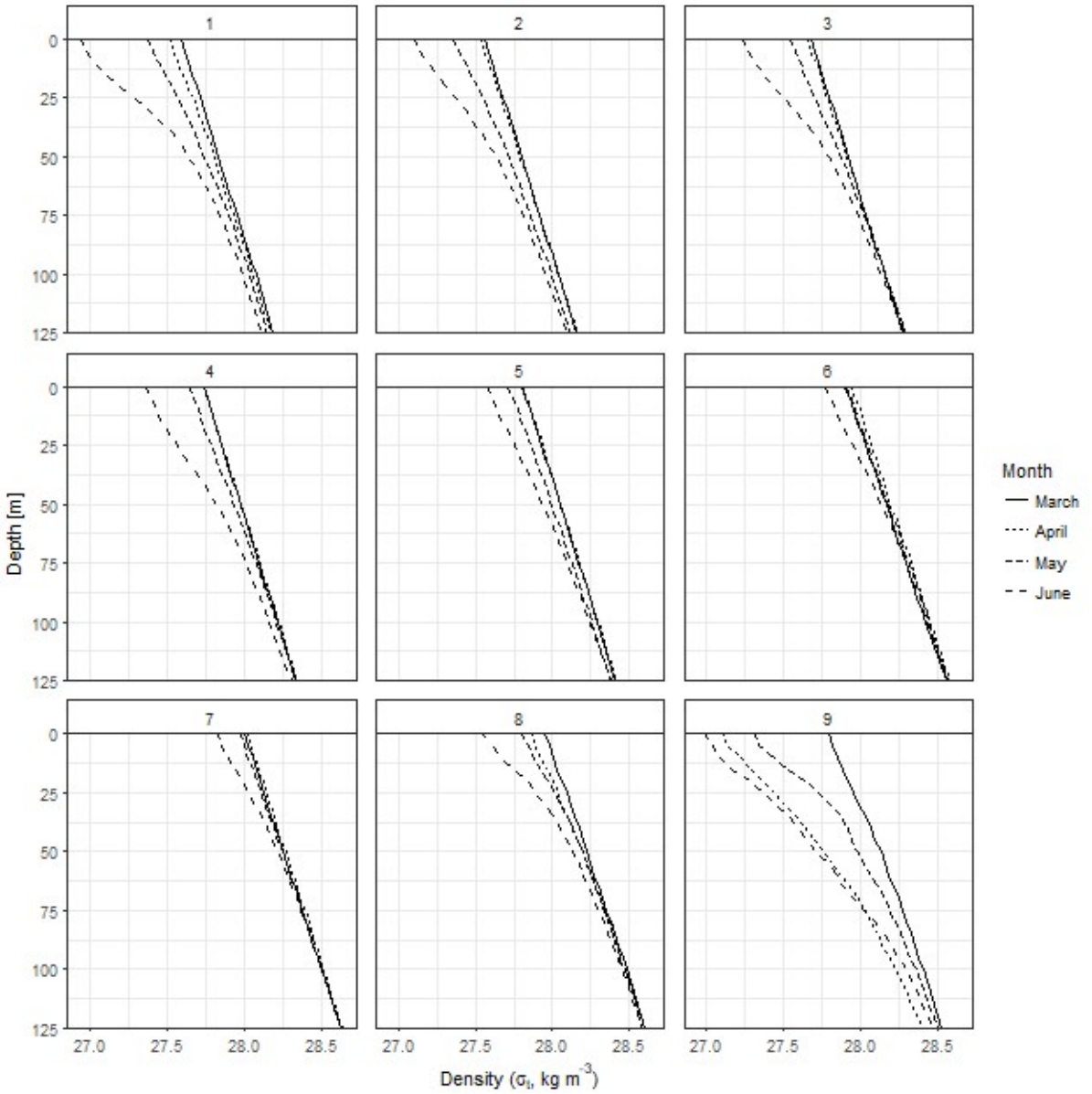

Figure 6: Comparison of density profiles of four months averaged for 9 stations for 2.5° intervals on a latitudinal gradient along 0.125°E (Data: World Ocean Atlas, Boyer et al. 2013).

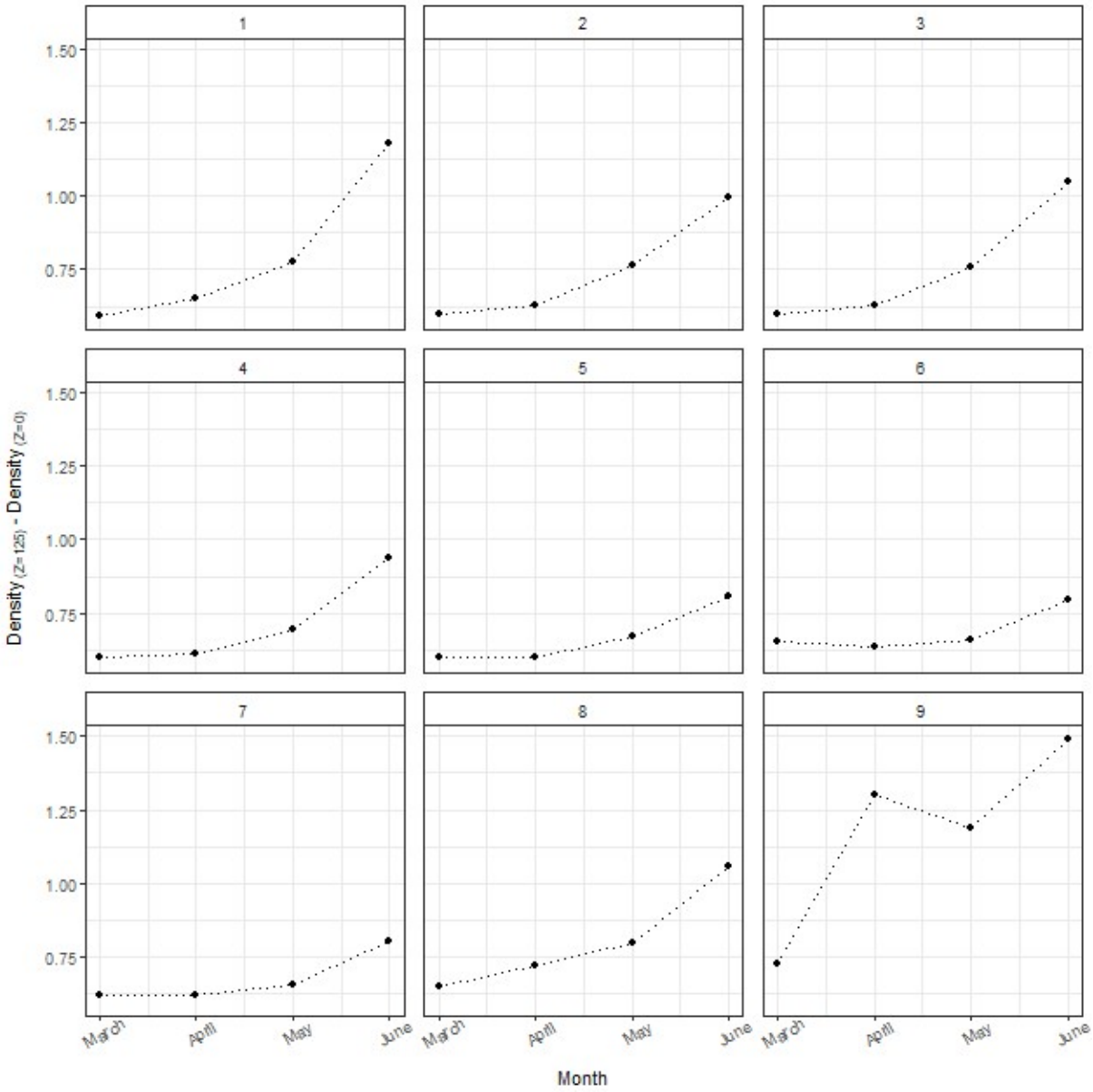

Figure 7: Difference between density at 125 m depth and the surface throughout spring for 9 stations.

3.4. Modelling of spring phytoplankton dynamics

Monthly turbulent diffusivities for stations 1-9 were calculated from density data (Table 3). Modelled population growth rates, peak heights and peak timing were markedly different between the nine stations, although chlorophyll concentrations and slope were similar for stations 1 – 8 after ca. day 100 of the simulation.

The first, although very slight increase in phytoplankton concentrations is observed at station 1. The other stations follow in order of latitude. Peak timing occurred in reverse order of latitude, with differences larger at higher latitudes. Growth rates and bloom magnitude increased with latitude. However, differences in peak height are larger at lower latitudes, while bloom magnitude of stations 8 and 9 are almost identical (Figure 8).

Diurnal variations in phytoplankton concentrations are clearly visible at lower latitudes (Figure 9). Surface layer nutrients are fully depleted earlier at higher latitudes. However, nutrients are depleted to similar concentrations and depth at all stations by the end of the simulation (Figure 10).

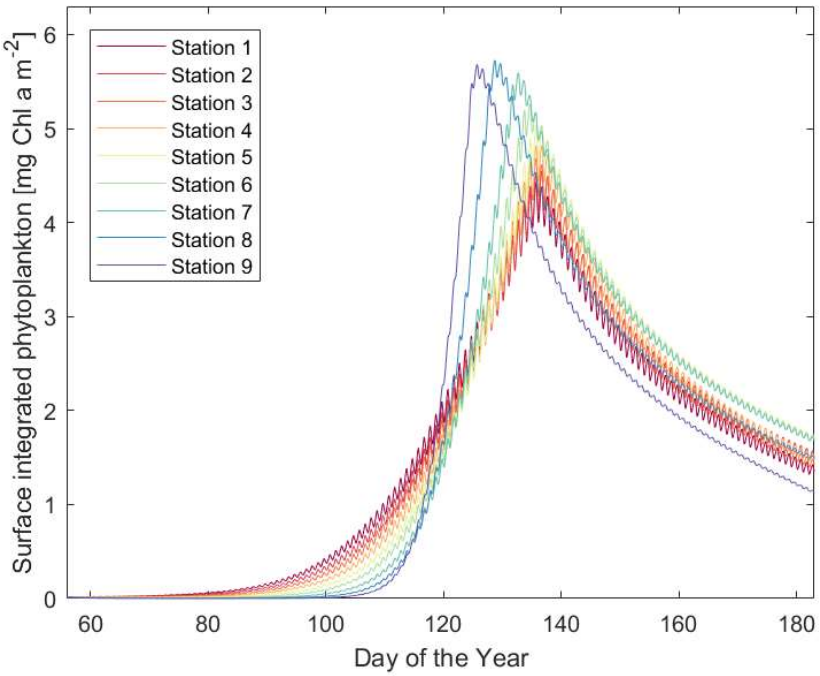

Figure 8: 127-day timeseries of chlorophyll concentrations integrated over the upper 25 m of a water column simulated for nine stations with monthly turbulent diffusivity values approximated from density stratification according to Equation 8, and hourly irradiance modeled in Astrocalc4R (Jacobson et al., 2011).

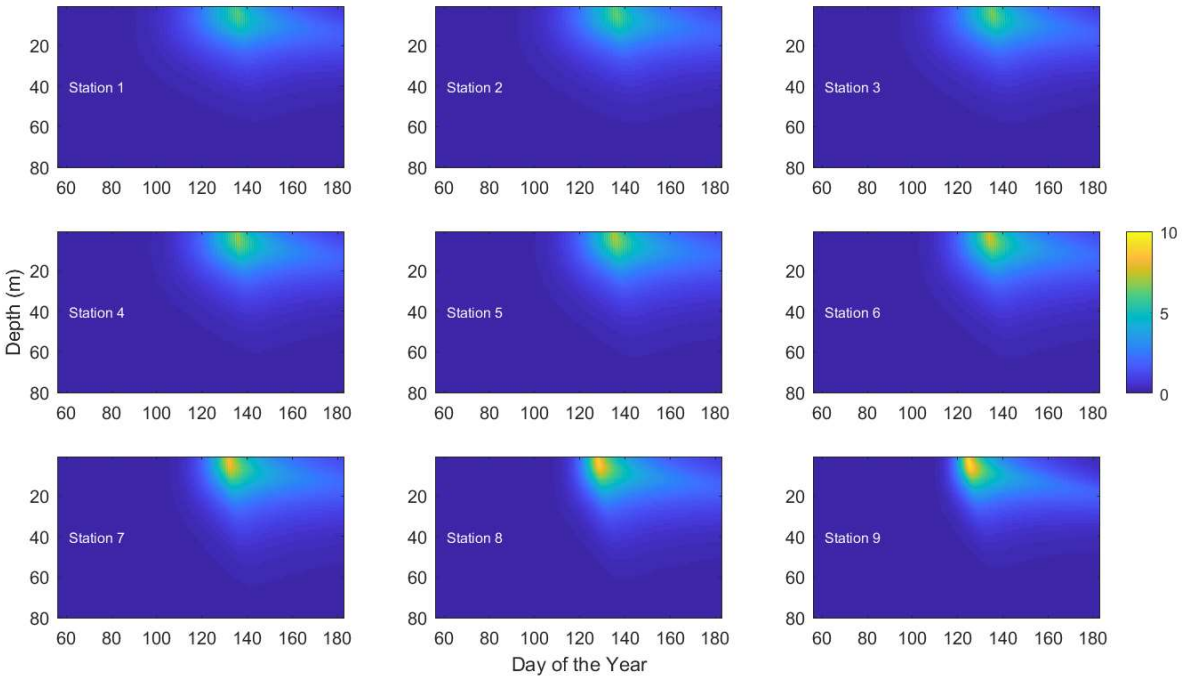

Figure 9: Phytoplankton concentrations (mg Chl a m^{-3}) simulated over 127 days using monthly turbulent diffusivity values approximated from density stratification according to Equation 8, and hourly irradiance modeled in Astrocalc4R (Jacobson et al., 2011).

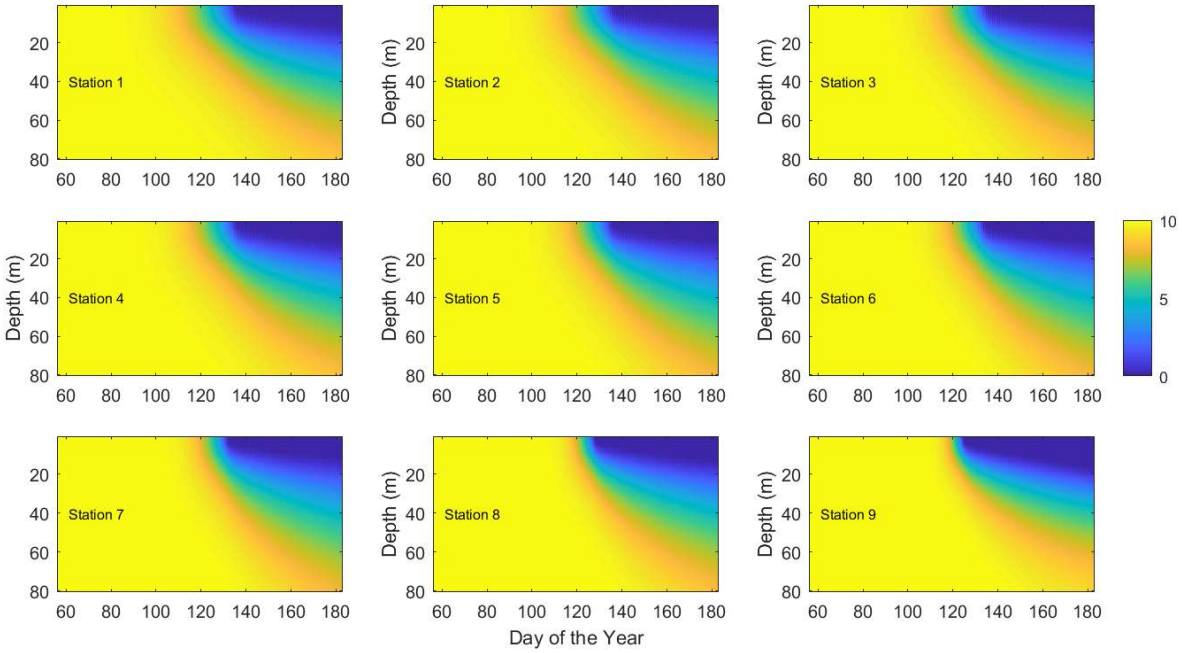

Figure 10: Nutrient concentrations (mmol N m^{-3}) simulated over 127 days using monthly turbulent diffusivity values approximated from density stratification according to Equation 8, and hourly irradiance modeled in Astrocalc4R (Jacobson et al., 2011).

Table 3: Average turbulent diffusivity [m^2 s^{-1}] of the upper 125 m at 5 stations for March-June, approximated from density stratification according to Equation 8.

Station \ Month	March	April	May	June
1	$5.094 \cdot 10^{-4}$	$4.602 \cdot 10^{-4}$	$3.852 \cdot 10^{-4}$	$2.85 \cdot 10^{-4}$
2	$5.128 \cdot 10^{-4}$	$4.897 \cdot 10^{-4}$	$3.999 \cdot 10^{-4}$	$3.165 \cdot 10^{-4}$
3	$5.178 \cdot 10^{-4}$	$4.892 \cdot 10^{-4}$	$4.036 \cdot 10^{-4}$	$3.024 \cdot 10^{-4}$
4	$5.106 \cdot 10^{-4}$	$4.992 \cdot 10^{-4}$	$4.398 \cdot 10^{-4}$	$3.285 \cdot 10^{-4}$
5	$5.080 \cdot 10^{-4}$	$5.088 \cdot 10^{-4}$	$4.528 \cdot 10^{-4}$	$3.771 \cdot 10^{-4}$
6	$4.713 \cdot 10^{-4}$	$4.824 \cdot 10^{-4}$	$4.591 \cdot 10^{-4}$	$3.801 \cdot 10^{-4}$
7	$4.963 \cdot 10^{-4}$	$4.936 \cdot 10^{-4}$	$4.671 \cdot 10^{-4}$	$3.845 \cdot 10^{-4}$
8	$4.739 \cdot 10^{-4}$	$4.198 \cdot 10^{-4}$	$3.859 \cdot 10^{-4}$	$3.088 \cdot 10^{-4}$
9	$4.200 \cdot 10^{-4}$	$2.503 \cdot 10^{-4}$	$2.911 \cdot 10^{-4}$	$2.082 \cdot 10^{-4}$

3.4.1. Modelled bloom timing

Bloom onset and maxima at all stations occurred within a period of 36 days in the model.

The correlation between bloom timing and latitude was statistically significant for three methods (Figure 11). Maximum chlorophyll concentrations occurred 0.5 days earlier per degree latitude. All other bloom timing methods detected a delay with latitude. Bloom onset as detected by the cumulative sum and 1 mg threshold method occurred respectively 0.34 and 0.16 days earlier per degree latitude. Exceptions were observed at stations 7 – 9, where onset advanced with increasing latitude.

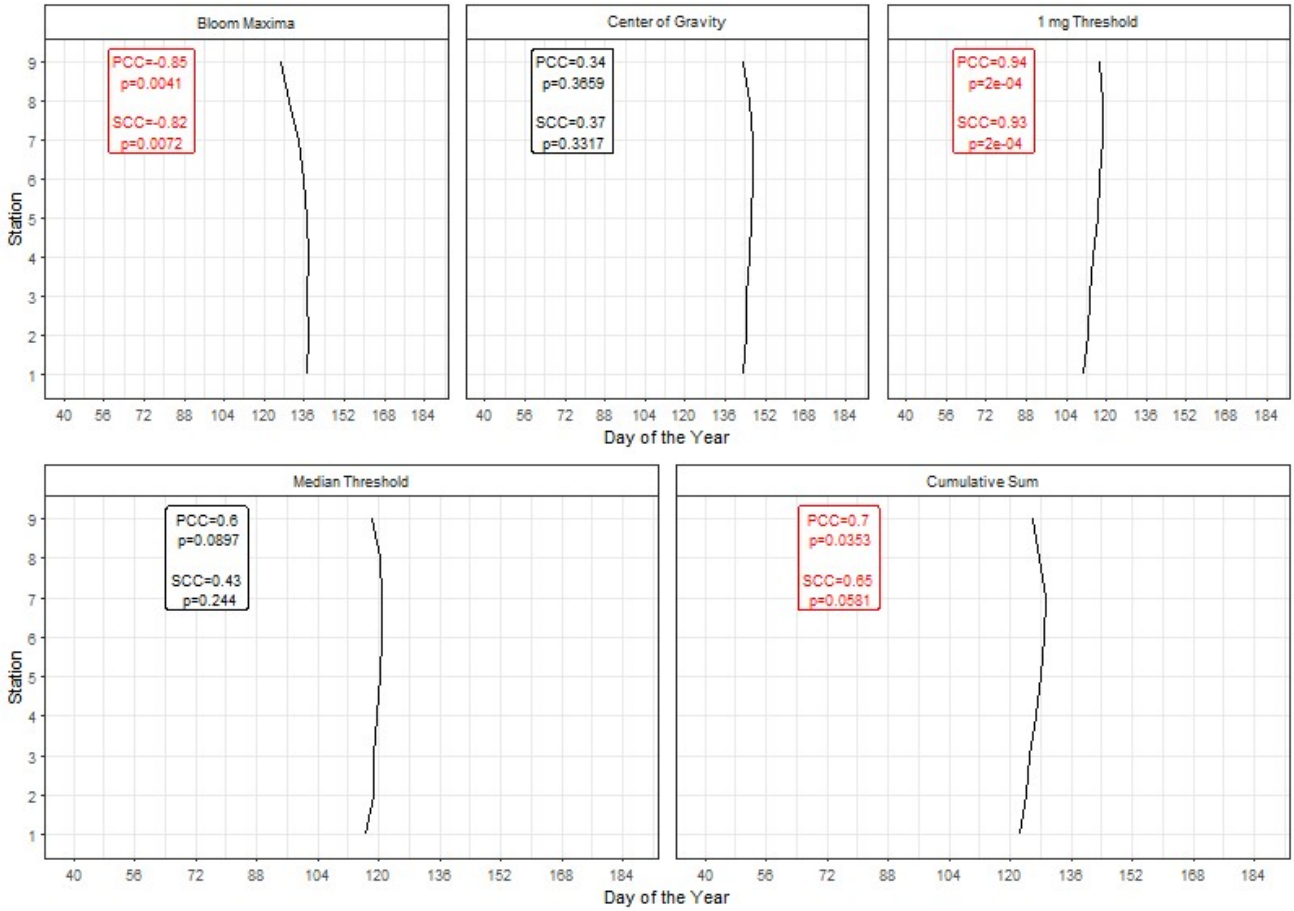

Figure 11: Bloom onset and maximum of modelled phytoplankton timeseries as identified by five different methods plotted against station number. Labels contain Pearson Correlation Coefficient (PCC), Spearman Rank Correlation Coefficient (SCC) and corresponding p-values, with statistically significant values ($p<0.05$) marked in red. Time is given as day of the year, with January 1st as day 1.

3.5. Sensitivity analyses

3.5.1. Turbulent diffusivity

Intense blooms were observed for the first three values of κ ($1.7 \cdot 10^{-4}$ m^2 s^{-1}, estimated as an average value for vertical mixing through the oceanic thermocline in Li et al., 1984, as well as values of an order of magnitude above and below). Increasing κ in this range led to an increase of surface chlorophyll maxima concentrations, but also to also to a delay in the timing of those maxima (Figure 12). Decreasing κ resulted in upper layer chlorophyll concentrations quickly approaching zero after peaking.

At low values of κ, nutrients in the upper water column are quickly depleted, resulting in a steep concentration gradient (Figure 14). The phytoplankton bloom deepens until limited by light (Figure 13). With higher turbulent diffusivities, nutrients are more quickly replenished from below and the bloom remains near the surface; however, it takes longer for a bloom to form.

When κ was increased by another order of magnitude by inserting the value derived from Equation 7, only a very slight increase in chlorophyll concentrations over time is recorded. Surface nutrient concentrations decrease accordingly, but are not nearly depleted by the end of the simulation (Figure 14).

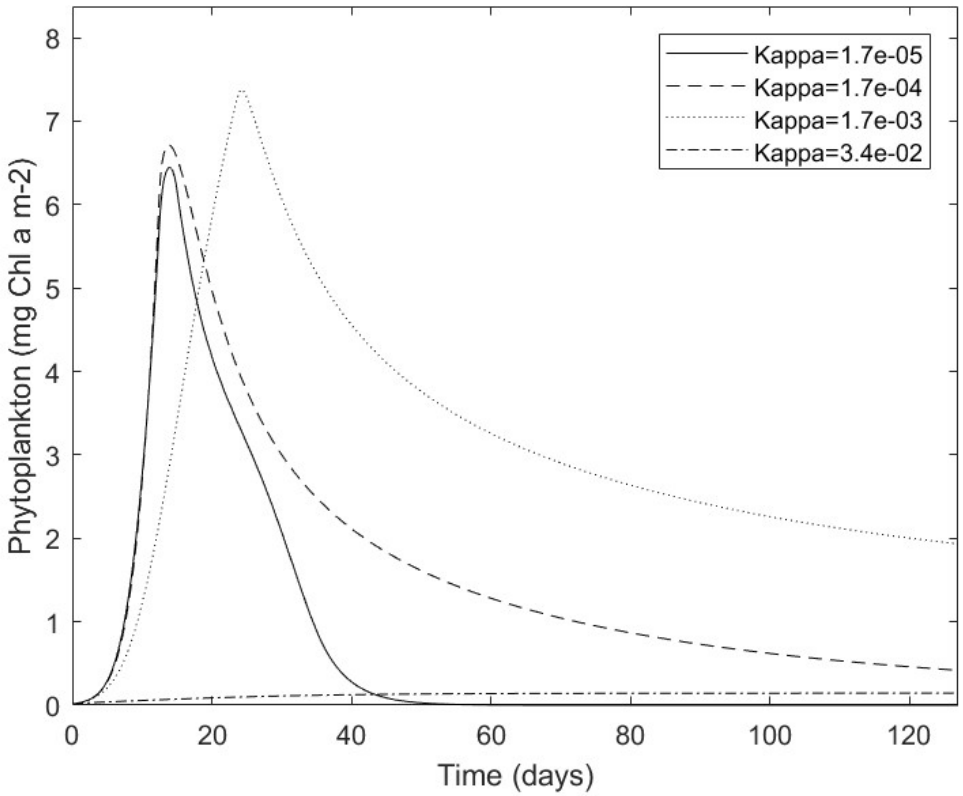

Figure 12: A 140-day timeseries of simulated Chl a integrated over the upper 25 m of a water column for three different values of κ (Turbulent diffusivity). Values for I_0 (600 mmol photons m^{-2} s^{-1}) and K_b (0.045 m^{-1}) were kept constant.

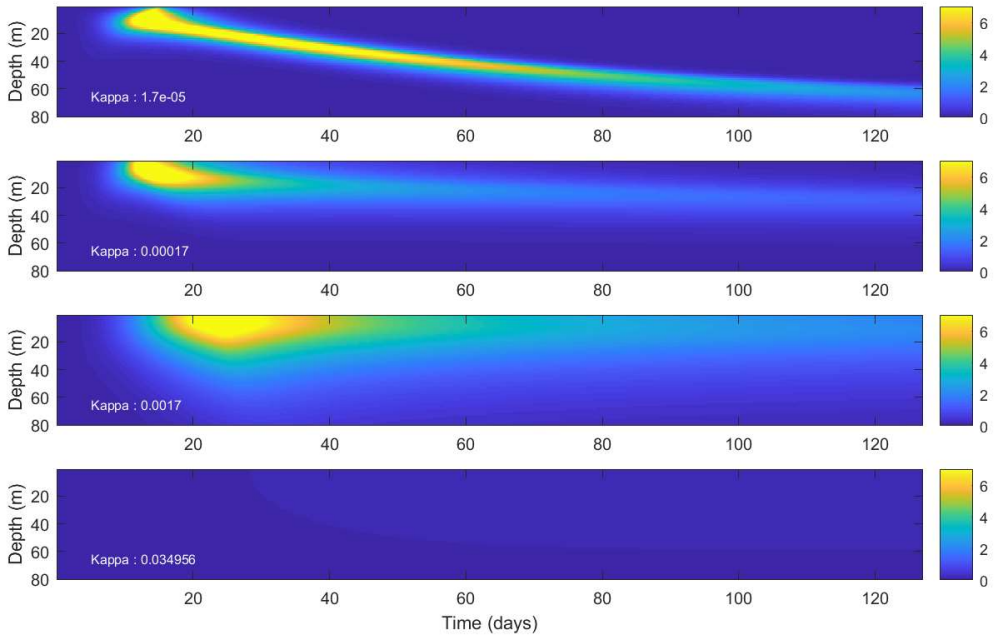

Figure 13: Chl a concentrations simulated over 140 days using four different values of κ (Turbulent diffusivity). Values for I_0 (600 mmol photons m^{-2} s^{-1}) and K_b (0.045 m^{-1}) were kept constant.

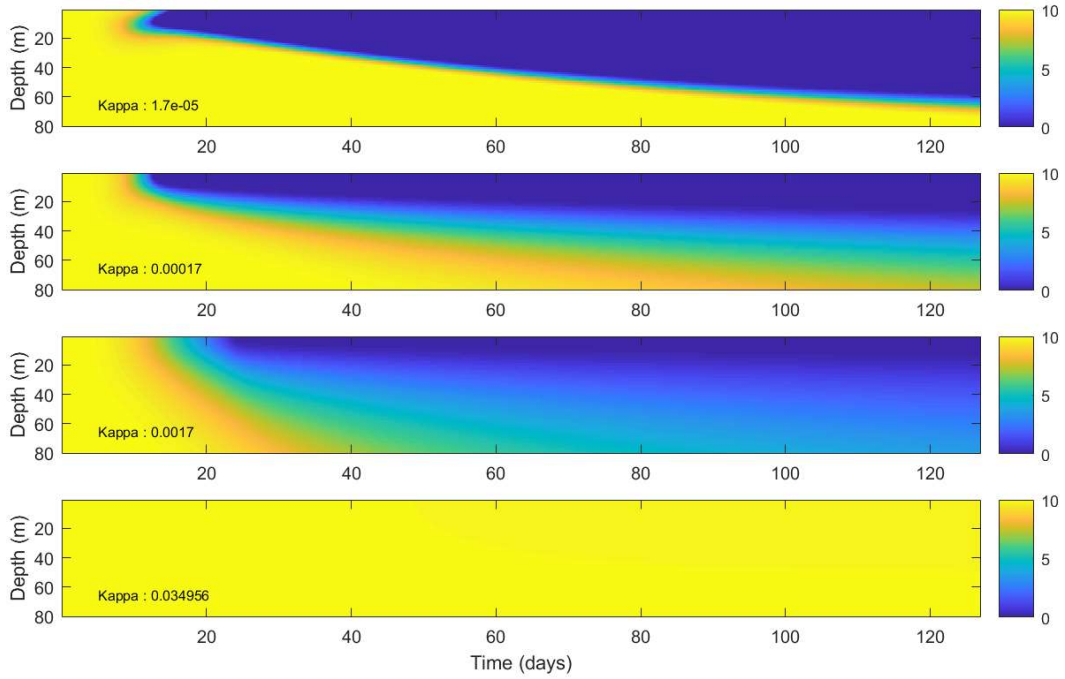

Figure 14: Nutrient concentrations (mmol N m^{-3}) simulated over 140 days using four different values of κ (Turbulent diffusivity). Values for I0 (600 mmol photons m^{-2} s^{-1}) and K_b (0.045 m^{-1}) were kept constant.

3.5.2. Irradiance

At a high-latitude light regime, bloom initiation is delayed compared to lower-latitude light regimes (Figure 15, Figure 16). However, bloom peak was reached slightly earlier at higher latitudes, and both peak chlorophyll concentrations and the growth rates leading up to them increase with station number. By the end of the simulation, chlorophyll concentrations are similar at all five light regimes, decreasing slightly with increasing latitude.

Diurnal increase and decrease in chlorophyll concentrations is clearly visible at low latitude light regimes (Figure 15, Figure 16). While chlorophyll concentrations begin to increase earlier at low latitude light regimes, maximum chlorophyll concentrations at all three light regimes almost coincide in time. The increase in chlorophyll concentrations and decrease in nutrient concentrations is steeper at higher latitude light regimes.

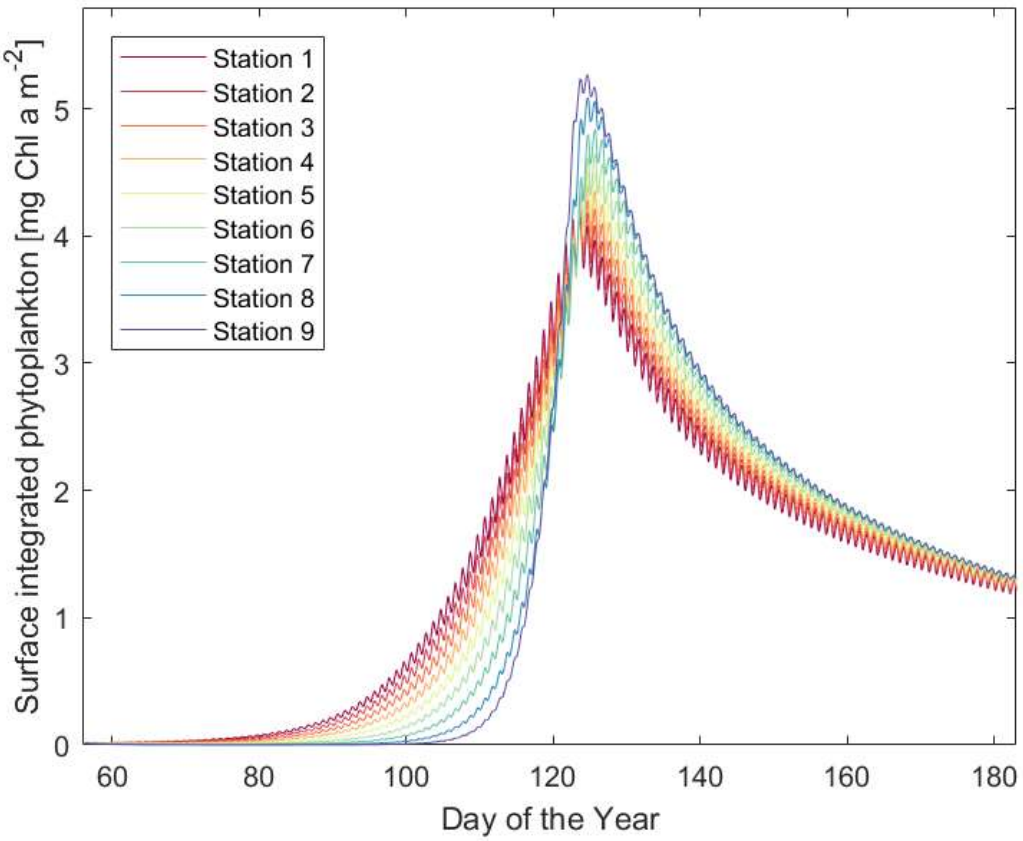

Figure 15: A 140-day timeseries of simulated Chl a integrated over the upper 25 m of a water column for light regimes modelled hourly for nine stations using the Astrocalc4R function (Jacobson et al., 2011). Values for κ ($1.7 \cdot 10^{-4}$ m^2 s^{-1}) and K_b (0.045 m^{-1}) were kept constant.

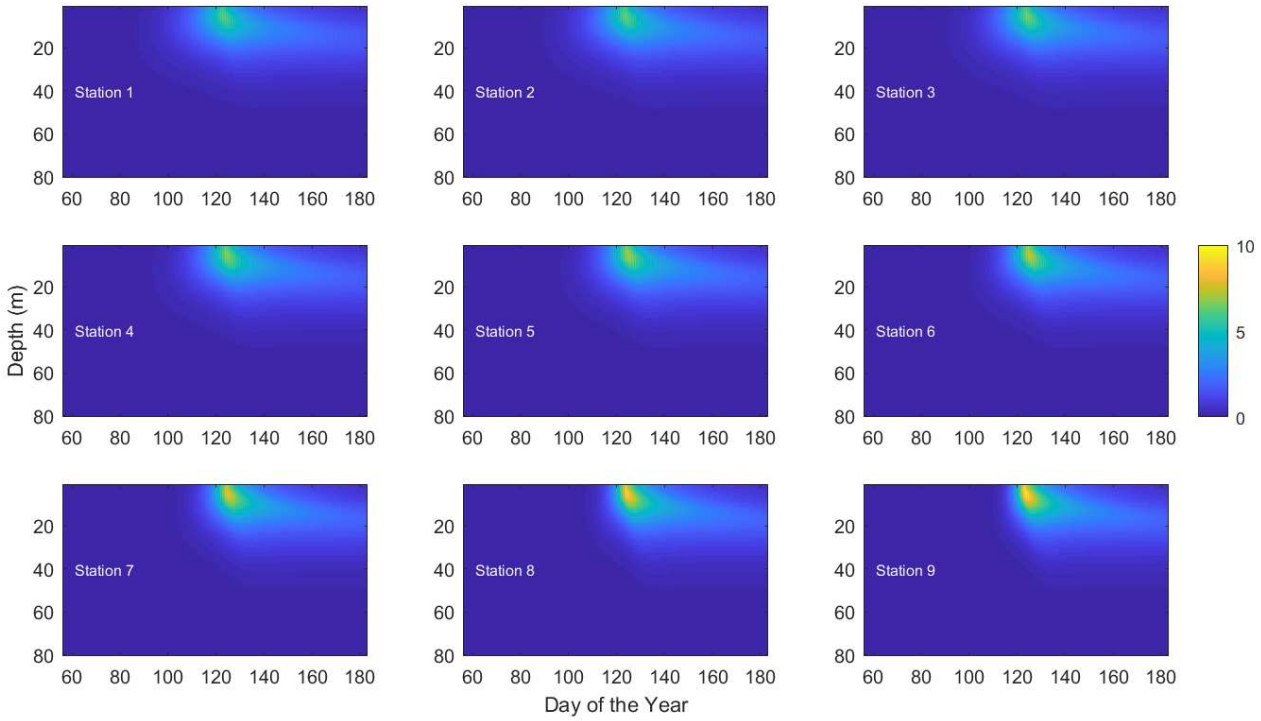

Figure 16: Chlorophyll concentrations (mg Chl m^{-3}) simulated over 140 days at light regimes modelled hourly for nine different latitudes using Astrocalc4R (Jacobson et al., 2011). Values for κ ($1.7 \cdot 10^{-4}$ m^2 s^{-1}) and K_b (0.045 m^{-1}) were kept constant.

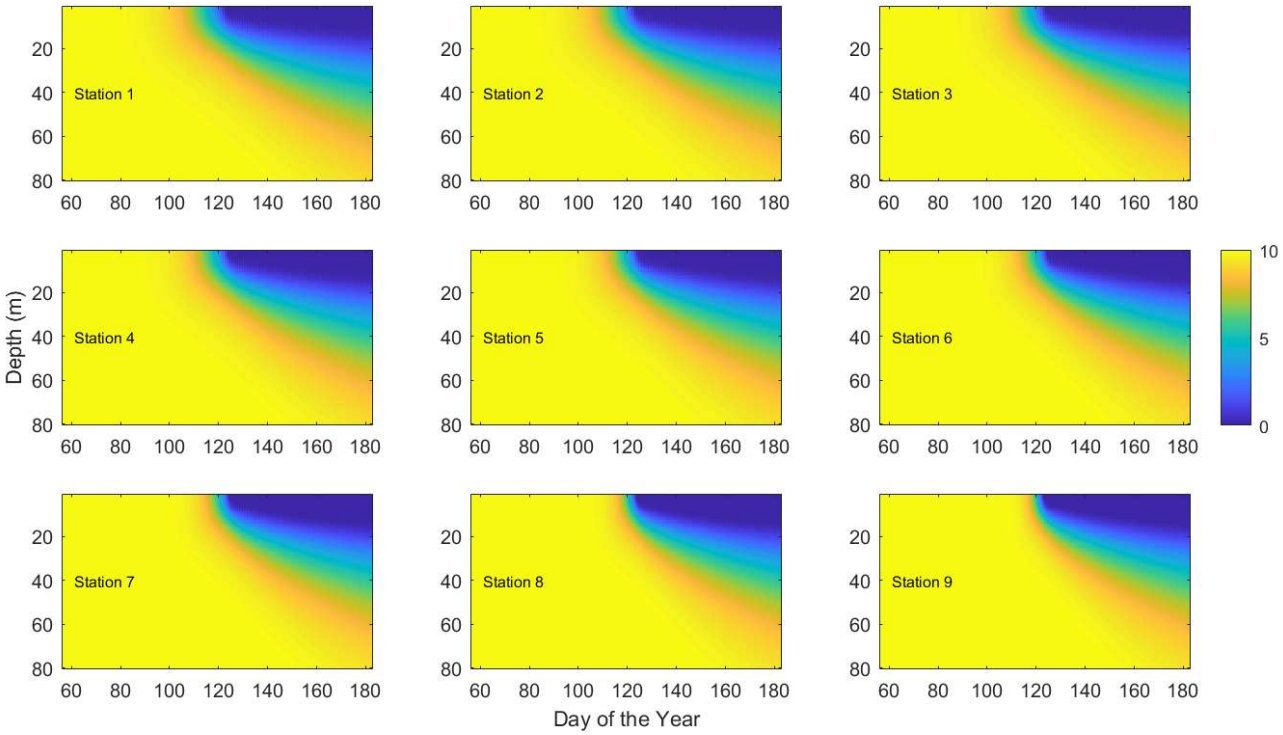

Figure 17: Nutrient concentrations (mmol N m^{-3}) simulated over 140 days at light regimes modelled hourly for nine different latitudes using Astrocalc4R (Jacobson et al., 2011). Values for κ ($1.7 \cdot 10^{-4}$ m^2 s^{-1}) and K_b (0.045 m^{-1}) were kept constant.

3.5.2.1. Bloom timing

Bloom onset as observed in the irradiance sensitivity analysis was delayed linearly with latitude, while timing of bloom maxima was not significantly correlated with station number (Figure 18).

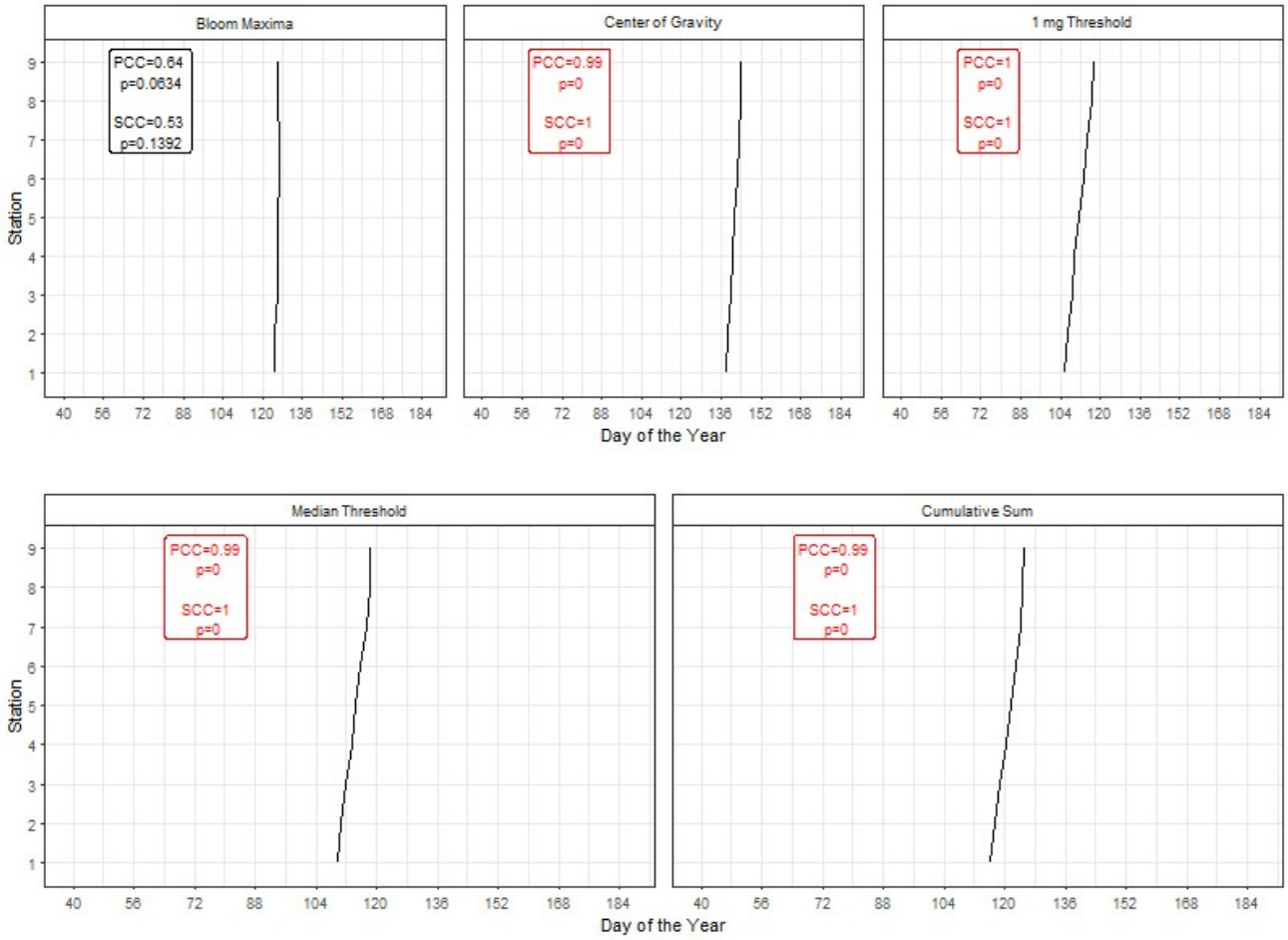

Figure 18: Bloom dates of chlorophyll timeseries modelled in an irradiance sensitivity analysis, as identified by four different methods, plotted against station number. Time is given as day of the year, with January 1st as day 1.

3.5.3. Background attenuation

Decreasing the background attenuation coefficient led to higher growth rates and peak chlorophyll concentrations in the upper 25 m of a water column, but also to a faster decrease of concentrations in that layer following a bloom; for the lowest value of K_b, surface chlorophyll concentrations approached zero by the end of the simulation (Figure 19). While peak and final concentrations differed, chlorophyll concentration dynamics in the upper 25 m do not appear very sensitive to changes in background attenuation.

A clearer picture of the effect of background attenuation is visible when considering a larger portion of the water column.

Low values of K_b allowed for deep chlorophyll maxima following surface blooms (Figure 20). Nutrients are depleted at greater depths, and nutriclines are steeper (Figure 21).

At higher levels of background light attenuation, phytoplankton are more constrained to the uppermost water layer.

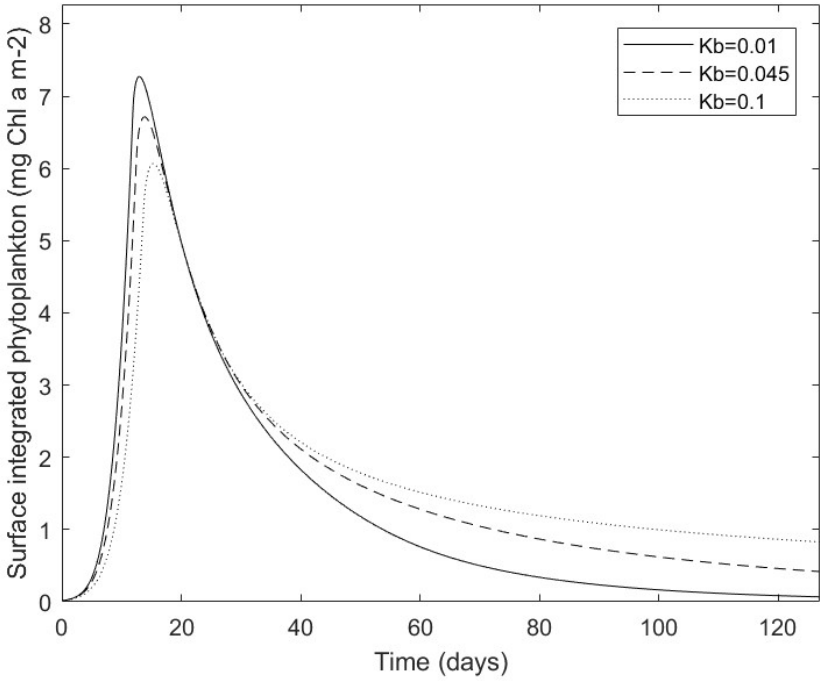

Figure 19: A 140-day timeseries of simulated Chl a integrated over the upper 25 m of a water column using three different values for K_b (background attenuation). Values for κ ($1.7 \cdot 10^{-4}$ m^2 s^{-1}) and I_0 (600 mmol photons m^{-2} s^{-1}) were kept constant.

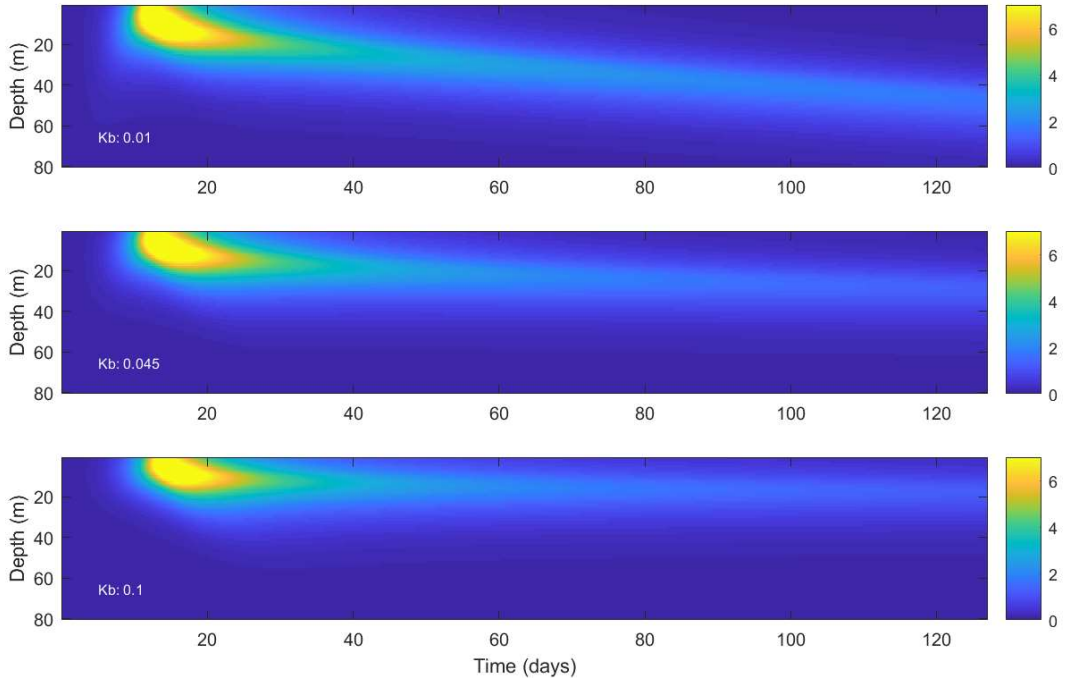

Figure 20: Chlorophyll concentrations (mg Chl a m^{-3}) simulated over 140 days using three different values of K_b (Background light attenuation). Values for κ ($1.7 \cdot 10^{-4}$ m^2 s^{-1}) and I_0 (600 mmol photons m^{-2} s^{-1}) were kept constant.

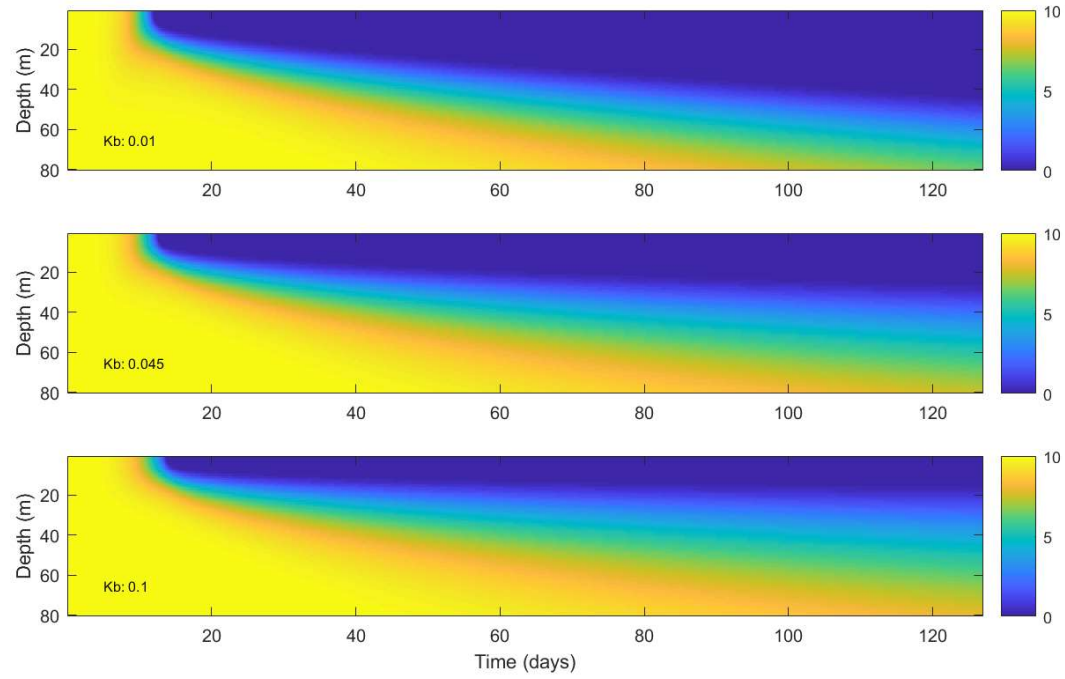

Figure 21: Nutrient concentrations (mmol N m^{-3}) simulated over 140 days using three different values of K_b (Background light attenuation). Values for κ ($1.7 \cdot 10^{-4}$ m^2 s^{-1}) and I_0 (600 mmol photons m^{-2} s^{-1}) were kept constant.

4. Discussion

Ocean color results suggest that spring blooms in the Nordic Seas follow a latitudinal pattern. A northward delay in bloom onset was observed between 60 and 75°N, but not at higher latitudes. Similar results in the idealized water column model indicate that this pattern can be explained by variation in the seasonality of density stratification and irradiance with latitude. Simulating an environment in which only light regimes differed with latitude led to a linear delay of bloom onset, and no correlation between timing of peak abundance and latitude. Blooms occurred earlier in this environment than one additionally governed by seasonal variation in vertical mixing.

Peak chlorophyll abundance in ocean color observations was highest at station 7 (75.125°N) (Figure 3). Peak abundances were higher at the northern and southern end of the latitudinal gradient than at stations in the middle.

Increasing levels of vertical mixing in the model produced blooms with delayed peaks of increased peak abundance within a range ($1.7 \cdot 10^{-5}$ $m^2 s^{-1}$ to $1.7 \cdot 10^{-3}$ $m^2 s^{-1}$) (Figure 11). Vertical mixing above that range did not produce blooms, but instead steady low-level production. Increased background attenuation led to lower and slightly delayed maximum chlorophyll concentrations (Figure 19). Surface concentrations at low background attenuations quickly decreased as deep chlorophyll maxima formed (Figure 19, Figure 20).

4.1. Limitations of the methods

4.1.1. Ocean color data

Remote sensing ocean color data, although a source of data on a global scale with high temporal resolution, is subject to several potential sources of bias. Sun glint and cloud cover lead to gaps in coverage, while water movement, e.g. white-capped waves, can obscure measurements. Coverage can be increased by merging data from multiple sensors, which was possible during almost the entire period covered in this study. Using 8-day composite datasets decreased temporal resolution, but also noise.

Measurements made at high solar zenith angles are excluded from ocean color datasets to avoid inaccuracies in atmospheric correction algorithms. This leads to long gaps in coverage of high latitudes in winter and early spring, explaining why timeseries of stations further north begin later in spring (Figure 2).

Cole et al. (2012) state that data gaps are longest and most frequent at high latitudes, mostly due to missing coverage in winter, although persistent cloud coverage over the North Atlantic and Arctic also plays a role. According to their study, this can lead to inaccuracies in bloom timing measures, e.g. the median threshold used here: missing data during early spring result in a median biased toward higher late spring and summer chlorophyll concentrations and therefore a higher threshold, and potentially later detection of bloom initiation. In the present study, this introduces the potential of even earlier bloom onset dates at high latitudes than the ones detected.

The ocean layer visible to sensors is rarely deeper than 25 m in oligotrophic water (Gordon & McCluney, 1975; Smith, 1981). With increased attenuation due to chlorophyll, the layer comprising most of the measured water-leaving radiance will be even shallower. Deep chlorophyll maxima, although widespread in oceans, are therefore invisible to remote measurements. Results of the sensitivity analyses performed in the present study suggest that

lower rates of vertical mixing, as are present in more stratified water columns, can lead to formation of steep nutriclines, with deep chlorophyll maxima following them. In the present study, such maxima are not accounted for.

At the northernmost station, sea ice affected ocean color measurements. Although light available for photosynthesis below the ice is limited, large under-ice phytoplankton blooms have been observed in previous studies even underneath pack ice (Arrigo et al, 2012). As these are not visible to ocean color sensors, bloom onset could have been misidentified.

4.1.2. Environmental variables

4.1.2.1. Irradiance

Irradiance was modelled as a function of solar position (Jacobson et al., 2011). Cloud cover was not accounted for, leading to overestimation of light available to facilitate growth in simulations. This assumes that cloud cover does not significantly differ with latitude at the stations analyzed in this study. Cloud cover is frequent and persistent above the North Atlantic, and less frequent, but more variable above the Arctic Ocean (Gregg & Casey, 2007; Wilson & Jetz, 2016).

4.1.2.2. Density stratification and turbulent diffusivity

Temperature and salinity data were obtained from the World Ocean Atlas database (Levitus et al., 2013).

The number of measurements included in each of these averages vary widely between stations and are especially low at the northern end of the latitudinal gradient. As most measurements were done during different scientific cruises, variation in methods and equipment used might have caused further discrepancies in data.

The method used here to approximate turbulent diffusivity is error prone in several ways. Constants a_1 and a_2 used in Equation 6 to compute dissipation rate of turbulent kinetic energy e are derived from a linear regression applied to measurements of e and corresponding wind speeds compiled from different studies, which sampled different depths and in one case, freshwater (Aksnes & Lie, 1990; Denman & Gargett, 1983). Further, wind speed in the same equation was assumed to be constant and identical at all stations, although seasonal and spatial variability is very likely.

In the model, average turbulent diffusivities of the upper 125 m were used, although turbulent diffusivity varies throughout the water column.

The values of turbulent diffusivity approximated from Equation 8 and used as to drive the model (section 3.5) are within the same order of magnitude as the one proposed by Li et al. (1984) (Table 4). Meanwhile, the value resulting from Equation 9, considering only wind speed, is two orders of magnitude larger.

A global average of mixing in the oceanic thermocline as the one proposed by Li et al. (1984) is unlikely to be representative for the upper water layer of the study area, while Equation 9 was derived from measurements taken throughout the mixed layer in the Nordic Seas (Sundby, 1983). The values approximated from Equation 8 might therefore be greatly underestimating actual mixing rates at the stations. A continuation of this study could focus on deriving spatially and seasonally resolved estimates of turbulent diffusivity from modelled or measured wind speeds, e.g. NOAA satellite wind speed measurements (H.-M. Zhang et al., 2006).

4.2. Drivers of latitudinal variation in bloom timing

Several studies have suggested a delay of bloom timing with latitude (Colebrook et al., 1984; Cushing, 1959; Siegel, 2002; Strass & Woods, 1988). Longhurst (1995) proposed that blooms in polar areas peak in summer rather than spring due to limited irradiance. The present study found an average delay of 4 days in bloom onset between stations below 75°N, similar to the 4 days detected by Wu et al. (2008) from 40-60°N in the Greenland Sea, and slightly lower than the delay of 6 days measured by Siegel et al. (2002) from 35°N-50°N in the North Atlantic. Siegel et al. (2002) found no relationship between bloom onset and latitude above 50°N, while Wu et al. (2008) found bloom onset north of 60°N coinciding with blooms at 40°N. Colebrook et al. (1984) and Strass & Woods (1988) both mention earlier blooms at high latitudes within their range of 40°-70°N. Similarly, the present study found a separate trend of earlier bloom times at higher latitudes north of 75°N. This was observed in ocean color measurements and reproduced in a simulation run with seasonally and latitudinally varying light and mixing regimes. Without latitudinal variation in mixing, bloom onset was instead linearly delayed along the whole latitudinal gradient. This suggests that irradiance is a main driver of the observed latitudinal delay below 75°N, counteracted by increased density stratification at the two northernmost stations. Wu et al. (2008), in a similar approach, reproduced such a bloom pattern in a model driven by mixed layer depth, supporting the conclusion that density stratification due to formation of a halocline facilitates early bloom onset at high latitudes.

Density stratification was strong at southern stations, then decreased toward the middle of the latitudinal gradient at ca. 70°N, and increased again towards the northernmost station at 80°N. Station 9 experienced the strongest seasonal increase in density stratification, while density stratification was low at stations 5 to 7, and varied little between months (Figure 6). In the south, stratification was due to thermocline formation (Appendix 2). Although the temporal resolution of the climatology developed for stations 1-9 in this study is not high, it is clearly visible that

station 9 was more strongly stratified than all other stations in April, while station 1 only reached similar levels of stratification in June (Figure 7). Between station 1 and station 9, bloom onset was delayed by ca. 20 days (Figure 4). This corresponds approximately to the time it took for irradiance at station 9 to reach similar levels to irradiance at station 1 (Figure 5). This suggests that bloom onset at station 9 was limited by irradiance.

Bloom onset estimates of simulated spring blooms occurred within a shorter timespan and slightly earlier than those observed in ocean color measurements. As the same observation was made in a seasonal environment with variation in irradiance and turbulent diffusivity and in the irradiance sensitivity analyses, this is likely due to an overestimation of available irradiance.

On average, bloom onset occurred 8 days earlier in the model, while bloom maxima occurred 24 days earlier. As the turbulent diffusivity sensitivity analysis also showed earlier blooms maxima at lower turbulent diffusivities, this might indicate that the values approximated from density stratification in this study are too low, and not representative of the study area.

Proximity to the coastline could be affecting ocean color and density stratification measurements. Station 1 is situated on the North Sea Shelf, and the area around it in which ocean color pixels were binned included the coastline of Shetland. Stations 8 and 9 are approximately 200 km removed from the west coast of Svalbard and might therefore be influenced by land run-off and topographically forced weather patterns that do not apply to stations in the open ocean. However, meltwater run-off in Svalbard does not start to a significant degree until July (Hodgkins, 1997). Proximity to the ice edge is therefore a more likely source of freshwater. At station 9, density stratification increased considerably between March and June due to decreased surface salinity (Appendix 3).

Stations 2-7 were all situated in the open ocean, well removed from terrestrial influence, and therefore perhaps better suited to show a latitudinal bloom pattern. Removing stations 1, 8 and 9 from the analysis slightly increased the correlation between bloom onset or maximum and latitude, but produced no change in statistical significance due to smaller sample size.

So far, this study has assumed that high chlorophyll concentrations at specific locations indicate blooms initiated by the favorable physical environment at these locations. However, transport of water masses from the North Atlantic into the Arctic takes place at rates of 9.5 ± 1.4 Sv (1 Sv = 106 m^3s^{-1}), with maximum velocities in spring (Fahrbach et al., 2001). A northward progression of ocean color bloom measurements could simply be due to advection of phytoplankton populations grown further south. While this might have contributed to the northward gradient visible at stations 1-7, the earlier bloom dates found at high latitudes suggest local initiation of blooms.

5. Conclusion

The findings of this study indicate that the date of spring bloom onset is correlated with latitude in the Nordic Seas, while chlorophyll maximum abundance and date of maximum abundance are not. Ocean color bloom observations showed later onset with latitude below 75°N, but earlier onset north of 75°N. Simulated blooms purely governed by latitudinal irradiance regimes were delayed with latitude along the entire study area, while simulations forced with turbulent diffusivity approximated from seasonally and latitudinally resolved density stratification led to patterns resembling those found in ocean color measurements. This indicates that latitudinal gradients in vertical mixing and irradiance drive latitudinal patterns of spring bloom timing, with vertical mixing at low latitudes reduced by temperature stratification, and mixing at high latitudes reduced by salinity stratification.

6. Acknowledgements

Thank you to Dag and Øystein, for reading many drafts and giving lots of valuable advice.

Thanks to everyone else who helped me with their advice, R and Matlab skills – among many others, Chris, Zoe and Richard.

I also want to acknowledge the Bergen Lesesal-crew. I hope we all manage to kick our new caffeine addictions. Thank you for always giving me valuable advice when I explained my problems to you (and myself), and thanks for not being mad at me usually doing the complete opposite. And in general, thanks for an awesome two years. You made Bergen my home! I can't wait to see you what you all end up doing, but I already know you will all be amazing at it.

Thank you to my Svalbardian friends. It was probably the best semester of my life, but definitely in the top eight. I am so glad I met you. Our friendship is the most significant result of this master thesis.

Thanks to the international girls, especially Petra and Angela. I will be so happy to see you again when we all emerge from the master-thesis tunnel.

Thanks to my family for everything. Not sure where I'm going from here, but it will probably be somewhere hard to reach again, and I hope you know it's not because I'm trying to avoid you. I couldn't do it if I didn't still feel your support even from far away!

And finally, thank you to Lena. I didn't acknowledge you in my Bachelor thesis, and I'm sorry. I wrote this entire master thesis just to fix that mistake. I hope you're happy now!

7. Bibliography

Aksnes, D. L., & Lie, U. (1990). A coupled physical-biological pelagic model of a shallow sill fjord. *Estuarine, Coastal and Shelf Science*, *31*(4), 459–486. https://doi.org/10.1016/0272-7714(90)90038-S

André, J.-M. (1992). Ocean color remote-sensing and the subsurface vertical structure of phytoplankton pigments. *Deep Sea Research Part A. Oceanographic Research Papers*, *39*(5), 763–779. https://doi.org/10.1016/0198-0149(92)90119-E

Atkins, W. (1928). Seasonal variations in the phosphate and silicate content of sea water during 1926 and 1927 in relation to the phytoplankton crop. *Journal of the Marine Biological Association*.

Behrenfeld, M. J. (2010). Abandoning Sverdrup's Critical Depth Hypothesis on phytoplankton blooms. *Ecology*, *91*(4), 977–989. https://doi.org/10.1890/09-1207.1

Blindheim, J., & Østerhus, S. (2005). The Nordic seas, main oceanographic features (pp. 11–37). American Geophysical Union (AGU). https://doi.org/10.1029/158GM03

Brody, S. R., Lozier, M. S., & Dunne, J. P. (2013). A comparison of methods to determine phytoplankton bloom initiation. *Journal of Geophysical Research: Oceans*, *118*(5), 2345–2357. https://doi.org/10.1002/jgrc.20167

Broms, C., & Melle, W. (2007). Seasonal development of Calanus finmarchicus in relation to phytoplankton bloom dynamics in the Norwegian Sea. *Deep-Sea Research Part II: Topical Studies in Oceanography*, *54*(23–26), 2760–2775. https://doi.org/10.1016/j.dsr2.2007.08.021

Cole, H., Henson, S., Martin, A., & Yool, A. (2012). Mind the gap: The impact of missing data on the calculation of phytoplankton phenology metrics. *Journal of Geophysical Research: Oceans*, *117*(8), 2–9. https://doi.org/10.1029/2012JC008249

Colebrook, J. M. (1979). MARINE BIOLOGY Continuous Plankton Records: Seasonal Cycles of Phytoplankton and Copepods in the North Atlantic Ocean and the North Sea. *Marine Biology*, *51*, 23–32.

Colebrook, J. M., Robinson, G. A., Hunt, H. G., Roskell, J., John, A. W. G., Bottrell, H. H., … Halliday, N. C. (1984). Continuous Plankton Records: a possible reversal in the downward trend in the abundance of the plankton of the North Sea and the Northeast Atlantic. *ICES*

Journal of Marine Science, *41*(3), 304–306. https://doi.org/10.1093/icesjms/41.3.304

Cushing, D. H. (1959). The seasonal variation in oceanic production as a problem in population dynamics. *ICES Journal of Marine Science*, *24*(3), 455–464. https://doi.org/doi:10.1093/icesjms/24.3.455

Cushing, D. H. (1990). Plankton Production and Year-class Strength in Fish Populations: an Update of the Match/Mismatch Hypothesis. *Advances in Marine Biology*, *26*, 249–293. https://doi.org/10.1016/S0065-2881(08)60202-3

Denman, K. L., & Gargett, A. E. (1983). Time and space scales of vertical mixing and advection of phytoplankton in the upper ocean. *Limnology and Oceanography*, *28*(5), 801–815. https://doi.org/10.4319/lo.1983.28.5.0801

Edwards, M., & Richardson, A. J. (2004). Impact of climate change on marine pelagic phenology and trophic mismatch. *Nature*, *430*(7002), 881–884. https://doi.org/10.1038/nature02808

Eilertsen, H., Sandberg, S., & Tøllefsen, H. (1995). Photoperiodic control of diatom spore growth: a theory to explain the onset of phytoplankton blooms. *Marine Ecology Progress*.

Fahrbach, E., Meincke, J., Østerhus, S., Rohardt, G., Schauer, U., Tverberg, V., & Verduin, J. (2001). Direct measurements of volume transports through Fram Strait. *Polar Research*, *20*(2), 217–224. https://doi.org/10.1111/j.1751-8369.2001.tb00059.x

Frouin, R., Lingner, D. W., Gautier, C., Baker, K. S., & Smith, R. C. (1989). A simple analytical formula to compute clear sky total and photosynthetically available solar irradiance at the ocean surface. *Journal of Geophysical Research*, *94*(C7), 9731. https://doi.org/10.1029/JC094iC07p09731

Garcia, H. E., Locarnini, R. A., Boyer, T. P., Antonov, J. I., Baranova, O. K., Zweng, M. M., … Johnson, D. R. (2013). World Ocean Atlas 2013, Volume 4: Dissolved Inorganic Nutrients (phosphate, nitrate, silicate) In: Levitus S. *Mishonov A., Editors*, *76*, 25.

Gordon, H., & McCluney, W. (1975). Estimation of the Depth of Sunlight Penetration in the Sea for Remote Sensing. *Applied Optics*.

Gran, H. H., & Braarud, T. (1935). A Quantitative Study of the Phytoplankton in the Bay of Fundy and the Gulf of Maine (including Observations on Hydrography, Chemistry and Turbidity). *Journal of the Biological Board of Canada*, *1*(5), 279–467. https://doi.org/10.1139/f35-012

Gregg, W. W., & Casey, N. W. (2007). Sampling biases in MODIS and SeaWiFS ocean chlorophyll data. *Remote Sensing of Environment*, *111*(1), 25–35. https://doi.org/10.1016/J.RSE.2007.03.008

Greve, W., Lange, U., Reiners, E., & Nast, J. (2001). Predicting the Seasonality of North Sea Zooplankton.

Henson, S. A., Robinson, I., Allen, J. T., & Waniek, J. J. (2006). Effect of meteorological conditions on interannual variability in timing and magnitude of the spring bloom in the Irminger Basin, North Atlantic. *Deep-Sea Research Part I: Oceanographic Research Papers*, *53*(10), 1601–1615. https://doi.org/10.1016/j.dsr.2006.07.009

Hodgkins, R. (1997). Glacier hydrology in Svalbard, Norwegian high arctic. *Quaternary Science Reviews*, *16*(9), 957–973. https://doi.org/10.1016/S0277-3791(97)00032-2

Howarth, R. W. (1988). Nutrient Limitation of Net Primary Production in Marine Ecosystems. *Annual Review of Ecology and Systematics*, *19*(1), 89–110. https://doi.org/10.1146/annurev.es.19.110188.000513

Huisman, J., Pham Thi, N. N., Karl, D. M., & Sommeijer, B. (2006). Reduced mixing generates oscillations and chaos in the oceanic deep chlorophyll maximum. *Nature*, *439*(7074), 322–325. https://doi.org/10.1038/nature04245

Huisman, J., Van Oostveen, P., & Weissing, F. J. (1999). Species Dynamics in Phytoplankton Blooms: Incomplete Mixing and Competition for Light. *The American Naturalist*, *154*(1), 46–68. https://doi.org/10.1086/303220

Jacobson, L. D., Seaver, A., & Tang, J. (2011). AstroCalc4R : software to calculate solar zenith angle; time at sunrise, local noon, and sunset; and photosynthetically available radiation based on date, time, and location.

Kahru, M., Brotas, V., Manzano-Sarabia, M., & Mitchell, B. G. (2011). Are phytoplankton blooms occurring earlier in the Arctic? *Global Change Biology*, *17*(4), 1733–1739. https://doi.org/10.1111/j.1365-2486.2010.02312.x

Korablev, A., Smirnov, A., & Baranova, O. K. (2014). Climatological Atlas of the Nordic Seas and Northern North Atlantic: NOAA Atlas NESDIS 77, *13*(June). https://doi.org/10.7289/V54B2Z78

Laevastu, T. (1962). *Water types in the North Sea and their characteristics*.

Levitus, S., Antonov, J. I., Baranova, O. K., Boyer, T. P., Coleman, C. L., Garcia, H. E., … Zweng, M. M. (2013). THE WORLD OCEAN DATABASE.

Li, Y., Peng, T. -H, Broecker, W. S., & Östlund, H. G. (1984). The average vertical mixing coefficient for the oceanic thermocline. *Tellus B*, *36 B*(3), 212–217. https://doi.org/10.1111/j.1600-0889.1984.tb00243.x

Longhurst, A. R. (1998). *Ecological geography of the sea*. Academic Press.

Mackas, D. L., Greve, W., Edwards, M., Chiba, S., Tadokoro, K., Eloire, D., … Peluso, T. (2012). Changing zooplankton seasonality in a changing ocean: Comparing time series of zooplankton phenology. *Progress in Oceanography*, *97–100*, 31–62. https://doi.org/10.1016/J.POCEAN.2011.11.005

Mann, K. H., & Lazier, J. R. N. (2013). *Dynamics of marine ecosystems: biological – physical interactions in the oceans* (Vol. 155). John Wiley & Sons.

Maritorena, S., & Siegel, D. A. (2005). Consistent merging of satellite ocean color data sets using a bio-optical model. *Remote Sensing of Environment*, *94*(4), 429–440. https://doi.org/10.1016/J.RSE.2004.08.014

Marshall, S., & Orr, A. (1928). The photosynthesis of diatom cultures in the sea. *Journal of the Marine Biological Association*.

Morel, A. (1988). Optical modeling of the upper ocean in relation to its biogenous matter content (case I waters). *Journal of Geophysical Research*, *93*(C9), 10749. https://doi.org/10.1029/JC093iC09p10749

Norheim, E., Klevjer, T., & Aksnes, D. (2016). Evidence for light-controlled migration amplitude of a sound scattering layer in the Norwegian Sea. *Marine Ecology Progress Series*, *551*, 45–52. https://doi.org/10.3354/meps11731

O'Reilly, J. E., Maritorena, S., Mitchell, B. G., Siegel, D. A., Carder, K. L., Garver, S. A., … McClain, C. (1998). Ocean color chlorophyll algorithms for SeaWiFS. *Journal of Geophysical Research: Oceans*, *103*(C11), 24937–24953. https://doi.org/10.1029/98JC02160

Platt, T., Fuentes-Yaco, C., & Frank, K. T. (2003). Spring algal bloom and larval fish survival. *Nature*, *423*(6938), 398–399. https://doi.org/10.1038/423398b

Racault, M. F., Le Quere, C., Buitenhuis, E., Sathyendranath, S., & Platt, T. (2012). Phytoplankton phenology in the global ocean. *Ecological Indicators*, *14*(1), 152–163. https://doi.org/10.1016/j.ecolind.2011.07.010

Redfield, A. C. (1958). The biological control of chemical factors in the environment. *American Scientist*. Sigma Xi, The Scientific Research Honor Society. https://doi.org/10.2307/27827150

Robinson, I. S. (2004). *Measuring the oceans from space: the principles and methods of satellite oceanography*. Springer Science & Business Media.

Siegel, D. A. (2002). The North Atlantic Spring Phytoplankton Bloom and Sverdrup's Critical Depth Hypothesis. *Science*, *296*(5568), 730–733. https://doi.org/10.1126/science.1069174

Smith, R. C. (1981). Remote Senslng and Depth Distribution of Ocean Chlorophyll. *Marine Ecology Progress Series*, *5*, 359–361. https://doi.org/10.3354/meps005359

Strass, V., & Woods, J. D. (1988). Horizontal and Seasonal Variation of Density and Chlorophyll Profiles between the Azores and Greenland. In *Toward a Theory on Biological-Physical Interactions in the World Ocean* (pp. 113–136). Dordrecht: Springer Netherlands. https://doi.org/10.1007/978-94-009-3023-0_6

Sundby, S. (1983). A one-dimensional model for the vertical distribution of pelagic fish eggs in the mixed layer. *Deep-Sea Research*, *30*(6A), 645–661.

Sverdrup, H. U. (1953). On conditions for the vernal blooming of phytoplankton. *J. Cons. Int. Explor. Mer*, *18*(3), 287–295.

Talley, L., Pickard, G., Emery, W., & Swift, J. (2011). Descriptive physical oceanography: an introduction.

Thimijan, R. W., & Heins, R. D. (1983). Photometric, radiometric, and quantum light units of measure: a review of procedures for interconversion. *HortScience*, *18*(December), 818–822.

Townsend, D. W., Keller, M. D., Sieracki, M. E., & Ackleson, S. G. (1992). Spring phytoplankton blooms in the absence of vertical water column stratification. *Nature*, *360*(6399), 59–62. https://doi.org/10.1038/360059a0

Vikebø, F. B., Korosov, A., Stenevik, E. K., Husebø, Å., & Slotte, A. (2012). Spatio-temporal overlap of hatching in Norwegian spring-spawning herring and the spring phytoplankton bloom at available spawning substrata, *71*, 81–89. https://doi.org/10.1093/icesjms/fsr174

Wienke, S. M., & Cloern, J. E. (1987). The phytoplankton component of seston in San Francisco Bay. *Netherlands Journal of Sea Research*, *2133*(1).

Wilson, A. M., & Jetz, W. (2016). Remotely Sensed High-Resolution Global Cloud Dynamics for Predicting Ecosystem and Biodiversity Distributions. *PLOS Biology*, *14*(3), e1002415. https://doi.org/10.1371/journal.pbio.1002415

Wu, Y., Platt, T., Tang, C., & Sathyendranath, S. (2008). Regional differences in the timing of the spring bloom in the Labrador Sea.

Zhang, H.-M., Bates, J. J., & Reynolds, R. W. (2006). Assessment of composite global sampling: Sea surface wind speed. *Geophysical Research Letters*, *33*(17), L17714. https://doi.org/10.1029/2006GL027086

Zhang, R.-H., Chen, D., & Wang, G. (2011). Using Satellite Ocean Color Data to Derive an Empirical Model for the Penetration Depth of Solar Radiation (H_p) in the Tropical Pacific Ocean. *Journal of Atmospheric and Oceanic Technology*, *28*(7), 944–965. https://doi.org/10.1175/2011JTECHO797.1

Appendix

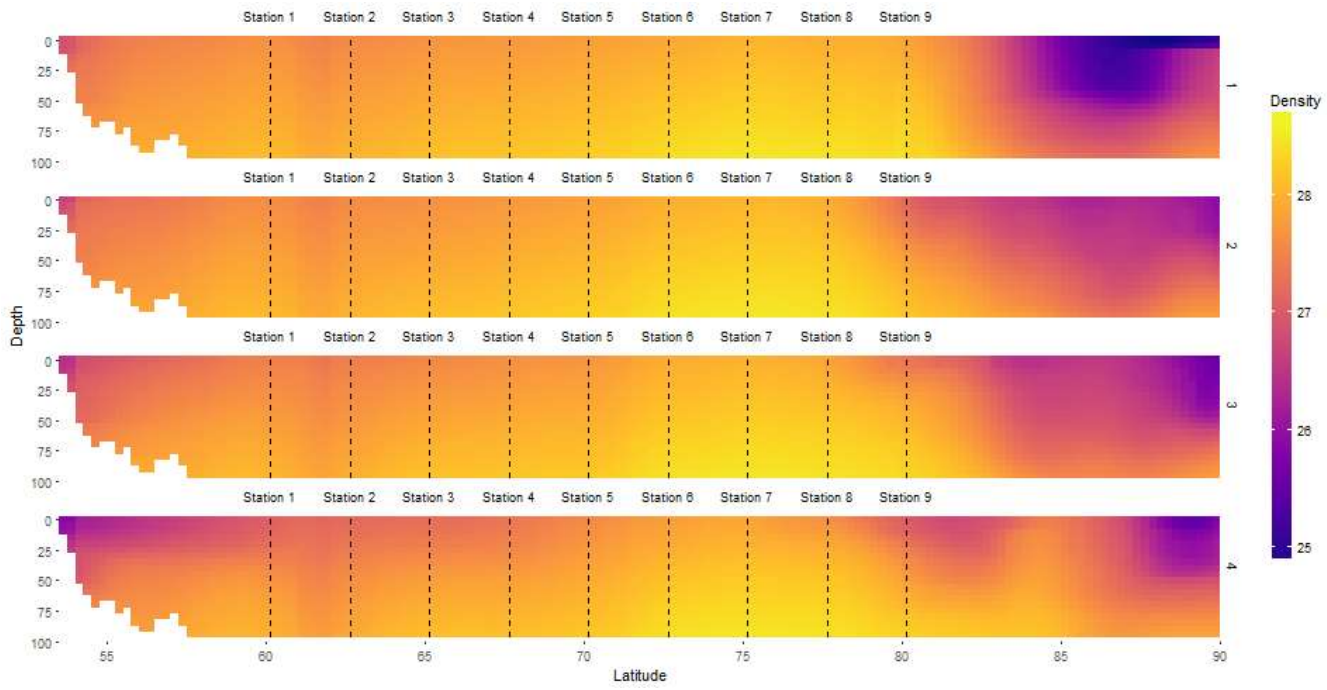

Appendix 1: Density sections computed from temperature and salinity data for March, April, May and June (Data: World Ocean Atlas) along 0.125°E, with stations 1-9 marked using dashed lines. Density data used in the dataset were taken during several different cruises between 2005-2012; some density profiles are the result of more than one measurement during this time period, while others were only measured once. All density profiles were interpolated to standard depths.

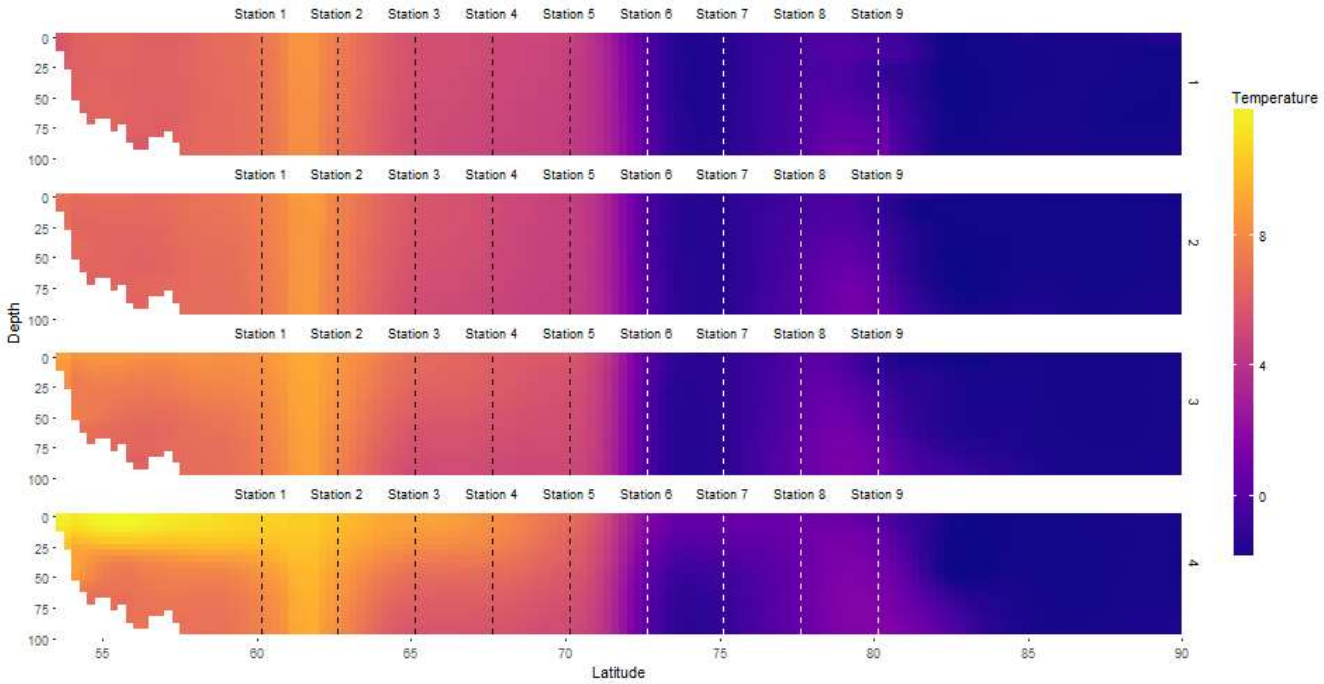

Appendix 2: Temperature sections for March, April, May and June (Data: World Ocean Atlas) along 0.125°E, with stations 1-9 marked using dashed lines. Density data used in the dataset were taken during several different cruises between 2005-2012; some temperature profiles are the result of more than one measurement during this time period, while others were only measured once. All temperature profiles were interpolated to standard depths.

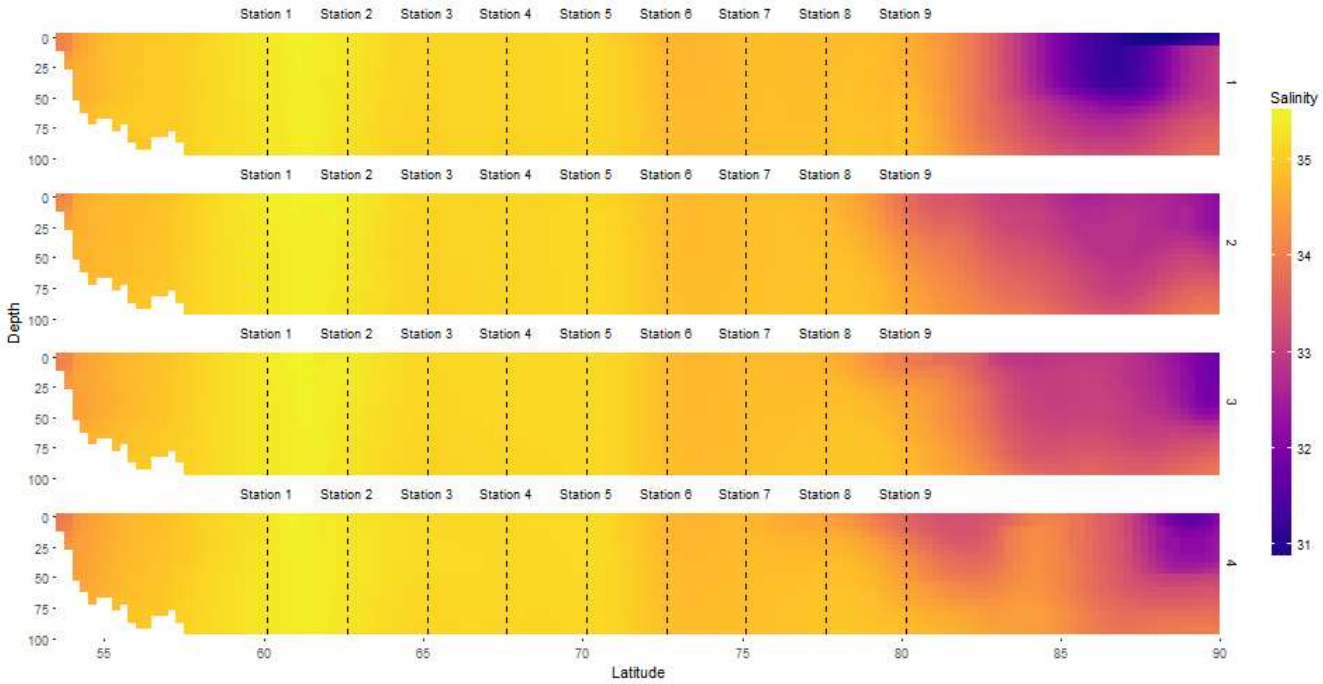

Appendix 3: Salinity sections for March, April, May and June (Data: World Ocean Atlas) along 0.125°E, with stations 1-9 marked using dashed lines. Salinity data used in the dataset were taken during several different cruises between 2005-2012; some salinity profiles are the result of more than one measurement during this time period, while others were only measured once. All salinity profiles were interpolated to standard depths.

Appendix 4: Matlab code for the idealized water column model.

```
%Phytoplankton model simular to that of Huisman et al.(2006)
clear all

% Temporal and spatial discretization
Z=300;        % Number of depth cells
DZ=1;         % Length of a depth cell (m)
T=182880;     %to fit with satellite data, modeled irradiance 26.2-3.7
DT=60;        % Length of a time step(s)
lon=0.125;
stations=1:1:9;
nroflocs=length(stations); %number of stations
%Water column properties
%Import turbulent diffusivity (m2 s-1) levels (average of each month)
%calculated from WOA density gradients at 5 different locations
klocs= importdata('klocs.txt');
klocs=(klocs.data)';
allklocs = interp1(0:45720:137160, klocs, 1:1:T, 'linear','extrap')'; %interpolate
to fit time steps

%%%%import modeled irradiance (astrocalc4r function in R package fishmethods) for
locations 1-5
allpar1=importdata('allpars.txt');
allpar1=(allpar1.data)';
allpar = interp1(1:60:T, allpar1, 1:1:T)';

Kb=0.045;      % Background light attenuation (m-1); as in Huisman et al. (2006)
NB=10;        % Fixed nutrient concentration in last depth cell (mmol N m-3)

%Phytoplankton traits as in Huisman et al (2006)
umax=1.11E-5; % Max growth rate (s-1)
m=2.78E-6;    % loss (death)rate (s-1)
Hi=20;        % Half saturation irradiance (micromol photons m-2 s-1)
Hn=0.025;     % Half saturation nutrient (mmol m-3)
K1=0.19;      % Self-shading factor, Morel 1988, converted to m2 mmol N-1 from m2
mg Chl-1
K2=0.428;
v=1.17E-5;    % Sinking velocity of phytoplankton (m s-1)
eps=0.5;      % Nutrient recycling coefficient

%Coefficients used to produce output from the simulation
CN=6.625;       % Carbon:Nitrogen Redfield ratio on mol basis
Cw=12;        % Molecular weigth of Carbon
CChl=50;      % Carbon to chlorophyll ratio


%Initialization of vectors
ST1=zeros(1,Z); %Phytoplankton growth
ST2=zeros(1,Z); %Phytoplankton mortality


surfacephy(1:nroflocs,1:T)=0;


for ksim=1:nroflocs
% New set of irradiance, turbulent diffusion for each location
kappa=allklocs(ksim,:);
I0=allpar(ksim,:);

%Initialization of water column state variables - homogenus distribution assumed
%as in pre-bloom winter situation
nit1(1:Z)=10;
phy1(1:Z)=0.01;
nit2=zeros(1,Z);
phy2=zeros(1,Z);
nitplot(1:Z,1:T)=0;
```

```
phyplot(1:Z,1:T)=0;
%Initialization of time and depth integrated phytoplankton growth
Pi=0;

%Note that both nutrients (nit1) and phytoplankton (phy1) are given in units
%of mmol N m-3 (Phytoplankton is given in units of cells m-3 in Huisman et al

% Coefficients that specify relative exchanges between depth cells during a time
step

R2=v*DT/DZ;      % The fraction of phytoplankton in a depth cell that sinks
                 % to the cell below during DT

%Assigning values to memory (for increased speed)
K = zeros(1,Z);
Iz = zeros(1,Z);

for tstep=1:T %Time loop
    %change kappa for each month
    S1=kappa(tstep)*DT/(DZ*DZ);% the fraction of a depth cell that is exchanged.
    %Update water column irradiance in first depth cell
    K=Kb+K1*(phy1(1)^K2);      %Light attenuation of first depth cell (surface)as
in Morel (1988)
    Iz(1)=I0(tstep)*exp(-K*DZ/2);   %Irradiance for each time step in first depth
cell (in middle of cell)
    %Update the other depth cells
    K(2:Z)=Kb+K1*(phy1(2:Z).^K2);
    Iz(2:Z)=Iz(1:Z-1).*exp(-K(2:Z)*DZ); %Irradiance

    %Update phytoplankton growth and loss terms for all dept cells
    Ilim=Iz./(Iz+Hi); %light limitation of depth cell
    Nlim=nit1./(nit1+Hn); %nutrient limitation of depth cell
    u=umax*min(Ilim,Nlim);     %phytoplankton growth rate
    ST1=u.*phy1*DT;           %Growth of phytoplankton during DT
    ST2=m*phy1*DT;           %Loss of phytoplankton during DT

    %Update first (surface) depth cell - no exchange through surface
    nit2(1)=nit1(1)*(1-S1)+nit1(2)*S1-ST1(1)+eps*ST2(1);
    phy2(1)=phy1(1)*(1-S1-R2)+phy1(2)*S1+ST1(1)-ST2(1);

    %Update last depth cell. Nutrient concentration is fixed in last cell!
    %Phytoplankton is not transported (by diffusion/sinking) below the last depth
cell.
    nit2(Z)=NB;
    phy2(Z)=phy1(Z)*(1-S1)+phy1(Z-1)*(S1+R2)+ST1(Z)-ST2(Z);

    %Update all the intermediate depth cells
    nit2(2:Z-1)=nit1(2:Z-1).*(1-S1-S1)+nit1(1:Z-2).*S1+nit1(3:Z)*S1-ST1(2:Z-
1)+eps*ST2(2:Z-1);
    phy2(2:Z-1)=phy1(2:Z-1).*(1-S1-S1-R2)+phy1(1:Z-
2).*(S1+R2)+phy1(3:Z)*S1+ST1(2:Z-1)-ST2(2:Z-1);

    %Store for figures
    nitplot(:,tstep)=nit2(:);
    phyplot(:,tstep)=phy2(:)*CN*Cw/CChl; %Convert to mg Chl m-3

    %Store accumulated phytoplankton growth (Pi)

    %Proceed to next time step with updated state variables
    nit1=nit2;
    phy1=phy2;
end

% Prepare values for plots
X=zeros(1,T);% preallocating for speed
totnit=zeros(1,T);
totphy=zeros(1,T);
for tstep=1:T
    X(tstep)=tstep*DT/(3600*24);   %Time-axis in days
```

```
    totnit(tstep)=sum(nitplot(:,tstep));
    totphy(tstep)=sum(phyplot(:,tstep));
end
for n=1:Z
    Y(n)=n*DZ;                      %Depth-axis in meters
end

%Plot figures

Nitrange=[0 10];
Phyrange=[0 10];

figure(1);
subplot(3,3,ksim)
imagesc(X+56,Y(1:80),nitplot(1:80,:),Nitrange);
hy=ylabel('Depth (m)');
text(5+56,40,['Station ' num2str(ksim)],'FontSize',8, 'Color','black');
colorbar

figure(2);
subplot(3,3,ksim)
imagesc(X+56,Y(1:80),phyplot(1:80,:),Phyrange);
hy=ylabel('Depth (m)');
text(5+56,40,['Station ' num2str(ksim)],'FontSize',8, 'Color','w');
colorbar

%Calculate surface integrated chlorophyll (Bi)
Bi=sum(phy1);
%Convert from mmol N m-2 to mg Chlorophyll + print
Bi=Bi*CN*Cw/CChl

%save integrated Chl from upper 25m for satellite comparison

upper25 = phyplot(1:25,:);
satcompare = mean(upper25,1);
surfacephy(ksim,:)=satcompare;

fname = sprintf('satcompare%d.txt', ksim);
fileID = fopen(fname, 'w');
fprintf(fileID,'%f\n',satcompare);
fclose(fileID);

end %ksim

figure(3);
plot(X+56,surfacephy(1:9,1:T))
set(gca,'Ylim',[0 1.1*max(surfacephy(:))]);
set(gca,'Xlim',[56 127+56]);

    xlabel('Day of the Year');%Write a label at X-axis
    ylabel('Surface integrated phytoplankton [mg Chl a m^-^2]', 'Interpreter',
'tex')
    legend(strcat("Station ",string(1:1:9)),'Location','NorthWest');
```